Applied Catalysis B: Environmental 237 (2018) 538–553

Contents lists available at ScienceDirect

Applied Catalysis B: Environmental

journal homepage: www.elsevier.com/locate/apcatb

Steam reforming of acetic acid over nickel-based catalysts: The intrinsic effects of nickel precursors on behaviors of nickel catalysts

Zhenjie Yu[a], Xun Hu[a,*], Peng Jia[a], Zhanming Zhang[a], Dehua Dong[a], Guangzhi Hu[b], Song Hu[c], Yi Wang[c], Jun Xiang[c,*]

[a] School of Materials Science and Engineering, University of Jinan, Jinan, 250022, China
[b] Key Laboratory of Chemistry of Plant Resources in Arid Regions, State Key Laboratory Basis of Xinjiang Indigenous Medicinal Plants Resource Utilization, Xinjiang Technical Institute of Physics and Chemistry, Chinese Academy of Sciences, Urumqi, 830011, China
[c] School of Energy and Power Engineering, Huazhong University of Science and Technology, Wuhan, 430074, China

ARTICLE INFO

Keywords:
Steam reforming
Acetic acid
Nickel precursors
Catalyst properties
Coke properties

ABSTRACT

The paper investigated the effects of various nickel precursors ($Ni(NO_3)_2$, $NiCl_2$, $NiSO_4$, $Ni(CH_3COO)_2$, $Ni(NH_2SO_3)_2$) on the catalytic behaviors of Ni/Al_2O_3 catalysts in steam reforming of acetic acid, aiming to understand the fundamental influences of nickel metal precursors. The catalysts were characterized with TPR, TPO, TPR-MS, TPO-MS, XRD, TG-MS, FT-IR, FT-Raman, BET method, element analysis, TEM and SEM. The results revealed the substantial influence of the nickel precursors on properties of Ni/Al_2O_3 catalysts. The use of $NiSO_4$ and $Ni(NH_2SO_3)_2$ as nickel precursors led to the low activities of the catalysts, due to the formation of Ni_3S_2 during reduction of the catalysts with hydrogen. The sulfur species were removed in the form of SO_2 during the calcination of the catalysts precursors in air and in the form of H_2S during the reduction of the calcined catalyst in hydrogen. $NiCl_2/Al_2O_3$ catalyst showed a negligible activity as the chlorine poisoned the catalyst and was difficult to be removed via calcination. Furthermore, chlorine could accelerate sintering of alumina. In comparison, $Ni(CH_3COO)_2$ as nickel precursor could effectively suppress the formation of $NiAl_2O_4$. $Ni(CH_3COO)_2/Al_2O_3$ catalyst showed comparable activity to that of $Ni(NO_3)_2/Al_2O_3$, but the resistivity towards coking was higher. In addition, the coke species produced over the catalysts have both large and small aromatic ring systems with the morphology of both amorphous and fibrous structures.

1. Introduction

Hydrogen is an important feedstock for synthesis of chemicals and a clean fuel for fuel cells, which can be produced from gasification of biomass or pyrolysis of biomass followed by steam reforming [1–12]. The pyrolysis of biomass produces a condensable product, bio–oil, which can be reformed with steam to produce hydrogen [13]. Nevertheless, steam reforming of bio–oil involves a complex reaction network and requires the full understanding of the reaction behaviors of the major components in bio–oil such as the carboxylic acids like acetic acid during steam reforming [14–19].

Although acetic acid is a simple organic compound, the steam reforming of acetic acid involves a complicated reaction network [20]. The effective reforming of acetic acid requires the development of active, selective and stable reforming catalyst [20–27]. The nickel–based catalysts such as Ni/Al_2O_3 has been widely investigated in steam reforming of acetic acid [21,28–30] or in the reforming of other organics or hydrogenation reactions [31,32]. The procedures for the preparation of the Ni/Al_2O_3 catalyst not only significantly affect the properties and performances of the catalysts [33–37], but also have varied environmental impacts.

Impregnation is a traditional method for preparation of the heterogeneous catalyst such as Ni/Al_2O_3. During the impregnation, nickel salt, dissolved in water or in organic solvent, is generally used as a precursor of nickel species [38,39]. Different nickel salts can be used and have been used to prepare the nickel catalysts. However, different nickel salt has different anion. Both nickel cation and the corresponding anion are co-impregnated on surface of carrier during impregnation.

Anion chelates with nickel ion, which might affect dispersion of nickel species during drying, calcination, and reduction of the catalyst. Further to this, the anion might be involved in the reforming reactions, modifying catalytic behaviors of the catalyst [40–43]. This is because the different anions such as Cl–, NO_3^-, CH_3COO–, SO_4^{2-} and NH_2SO_3– have different properties and distinct decomposition temperatures. They might interact with nickel cation or alumina carrier in different ways, which could potentially affect dispersion of nickel species,

* Corresponding authors.
E-mail addresses: Xun.Hu@outlook.com (X. Hu), xiangjun@hust.edu.cn (J. Xiang).

https://doi.org/10.1016/j.apcatb.2018.06.020
Received 25 January 2018; Received in revised form 30 May 2018; Accepted 6 June 2018
Available online 06 June 2018
0926-3373/ © 2018 Elsevier B.V. All rights reserved.

reduction of nickel oxides, and interaction of nickel with alumina. Further fundamental understanding about effects of anions on behaviors of nickel is required for the development of effective nickel-based catalysts.

In addition to the aspects about development of catalysts, environmental impact during manufacturing catalysts also deserves attention. The removal of these anions during the calcination or reduction of the catalysts could generate some pollutants such as NO_x, NH_3, SO_2 or H_2S. The emission of these gases should be considered during preparation of the catalysts to minimize environmental impact. In this study, in order to understand how the anions of nickel salts affect the properties of nickel species and how they involve in steam reforming reactions, the typical Ni/Al_2O_3 catalysts, prepared with $Ni(NO_3)_2$, $NiCl_2$, $NiSO_4$, $Ni(CH_3COO)_2$ or $Ni(NH_2SO_3)_2$, as the precursors of nickel, were characterized in detail and evaluated in steam reforming of acetic acid.

2. Experimental section

2.1. Materials

γ–A_2O_3 (specific area 257 m^2/g, pore volume 0.41 cm^3/g, mean pore size of 3.1 nm) was used as the support for the nickel catalysts. $Ni(NO_3)_2$, $NiCl_2$, $NiSO_4$, $Ni(CH_3COO)_2$, $Ni(NH_2SO_3)_2$, which are analytical grade, were used as the precursors of nickel.

2.2. Preparation of the catalysts

Ni/Al_2O_3 catalyst was prepared via an incipient wetness impregnation method. The aqueous solution of $Ni(NH_2SO_3)_2{\cdot}4H_2O$, $Ni(NO_3)_2{\cdot}6H_2O$, $NiCl_2{\cdot}6H_2O$, $Ni(CH_3COO)_2{\cdot}4H_2O$, or $NiSO_4{\cdot}6H_2O$ were prepared and used as the precursors of nickel. The dried γ–A_2O_3 were added to the solution and, the catalyst precursors were then dried at 120 °C for 24 h. The precursors were then further processed via three methods: In the first processing method, the catalyst precursors were reduced directly in a flowing hydrogen (60 ml min^{-1}) at 600 °C for 1 h, without the traditional calcination step. In the second processing method, the catalyst precursors were calcined at 600 °C for 4 h prior to the reduction. In the third processing method, the calcination temperature used was 900 °C. The catalysts processed via the different method will be specified in the text. The nickel loading (in metallic form) to alumina was 20 wt% for all the Ni/Al_2O_3 catalysts prepared.

2.3. Catalyst characterizations

The temperature–programmed reduction (TPR) of the calcined catalysts was performed in Vodo VD Sorb–91x instrument. The typical procedure was listed as follows: 20 mg of sample (precisely weighted) was loaded in a quartz reactor and was then heated to 105 °C under an Ar flow of 20 ml min^{-1} at 105 °C for 1 h in order to remove moisture absorbed on surface of the catalysts. After that, the catalyst was heated from 50 to 950 °C under a 5 vol.% H_2/Ar stream with the flow rate of 20 ml min^{-1}. TPR-MS was conducted via connecting the outlet of the Vodo VD Sorb–91x instrument with a mass spectrometer (MS) to monitor the gaseous products formed during the reduction.

H_2-TPD and NH_3-TPD was performed also by using the Vodo VD Sorb–91x instrument. For the H_2-TPD experiments, the catalyst sample after the calcination at 600 °C (ca. 50 mg but precisely weighted) was loaded and reduced at 600 °C with a 5 vol.% H_2/Ar (50 mL/min). The sample was then cooled to room temperature (25 °C) and the adsorption of hydrogen was conducted in a H_2 flow (50 mL/min) for 1 h. After that, the sample was swept with Ar until the baseline was leveled before heating to 900 °C with a ramping rate of 10 °C/min in an Ar flow (50 ml/min). The procedures for conducting the NH_3-TPD were basically similar to that of H_2-TPD. The main difference was that the catalyst sample was measured directly after the calcination. The adsorption of NH_3 was conducted at a room temperature under a 10 vol.% NH_3/Ar flow of 50 ml/min for 1 h. The desorption of NH_3 was performed from room temperature to 900 °C at a ramping rate of 10 °C/min in a helium flow (50 ml/min). The release of NH_3 was monitored with a TCD.

UV–vis diffuse reflectance spectra (UV–vis DRS) of the calcined catalysts were recorded by using a spectrometer (Persee, T9s) in a range of 200–800 nm. The sample was ground into powder and then tableted before the analysis. Alumina carrier was used as a reference material.

The surface areas of the catalysts were determined by N_2–desorption isotherms at –196 °C with Pioneer, SSA–6000 instrument. The surface areas were calculated by Brunauer–Emmett–Teller(BET) equation. The pores size distribution was determined by BJH method. Before the analysis, the sample was loaded and pretreated at 200 °C for 2 h for the adsorption and desorption of nitrogen.

Elemental analysis (EA) was performed by using Euro EA3000–Single instrument for determining composition of the organic elements (C、H、S、N) in the samples. During the analysis, the sample was heated in the instrument at 950 °C under an O_2/Ar flow of 100 ml·min^{-1}. The gaseous products formed were analyzed and the C, H, N and S elemental composition were calculated.

Thermo-gravimetric analysis (TG) were performed by using TG8121 Rigaku Corp instrument, aiming to analyze the coke and the weight change of the samples during heating. Before the analysis, the sample was pretreated at 105 °C for 10 min in order to remove the moisture absorbed. The sample was then heated to 900 °C at 10 °C min^{-1} under a N_2 flow of 50 ml min^{-1}. TG-MS was conducted via connecting the instrument with a mass spectrometer (MS) to monitor the formation of the gaseous products during the TG measurement.

X–Ray diffraction (XRD) characterization were performed with Philips X pert MPD instrument. The XRD patterns of the catalysts were recorded with a diffract meter operating at 40 kV and 100 mA, using a Cu–K α monochromatic X–ray source. The data with a Bragg angle (2Θ) of 10–80° were collected.

Raman spectra of the catalysts used in the stability tests were collected to analyze the aromatic ring structure of the coke formed by using Horiba LabRam HR Evolution instrument.

DRIFTS spectra were collected by using a Nicolet IS 500 FT-IR spectrum spectrometer equipped with a modified Harrick Praying Mantis DRIFT cell. The changes of the functional groups of the samples during heating in vacuum were measured. Before the analysis, the samples were ground uniformly, and pretreated at 60 °C in a vacuum oven for 12 h. The pretreated sample (0.5 g) was pressed into the cell. The temperature of the cell loaded with sample was then increased from 35 to 800 °C at a ramping rate of 10 °C/min. Background profiles were collected in a separated test at the different temperatures with an empty cell and then were deducted from the test results.

Temperature programmed oxidation (TPO) was conducted by using PCA–1200 instrument. Prior to the experiment, the sample was dried at 200 °C under a high–purity Ar gas flow to remove the absorbed moisture for 1 h. After that, 20 mg of catalyst was heated to 800 °C at a ramping rate of 15 °C/min in a 5% O_2/He flow (flow rate 20 ml/min). TPO-MS was conducted via connecting the instrument with a mass spectrometer (MS) to monitor the formation of the gaseous products during the oxidation of coke.

EDS–Mapping was conducted to analyze the distribution of Ni, Al and C elements by using FESEM, FEI, QUANTA FEG 250. The sample was dispersed in ethanol and sonicated into a uniform mixture. The distribution of Ni, Al, C elements in the microstructure of the material were then analyzed.

2.4. Catalytic tests

The catalytic performances of the catalysts were investigated in a fixed-bed continuous flow reactor. The catalyst (0.5 g) was loaded in a quartz reactor and was heated over a linear temperature ramp (20 °C min^{-1}) from 300 to 600 °C under a N_2 flow of 60 ml·min^{-1} with the

holding time of 30 min at each investigated temperature. The mixture of acetic acid/water was pumped into the quartz reactor with a liquid velocity of 0.12 ml min^{-1}. The gaseous products were analyzed by a GC fitted with TCD and FID detectors. The liquid products were collected in a condenser with icy water as coolant and were analyzed by a SHIMADZU LC-20 A liquid chromatography (LC).

The conversion of acetic acid was calculated according to the equation below:

$$\text{Cacid}(\%) = \frac{\text{Acetic acid in the feedstock - unreacted acid in the residual}}{\text{acid in the feedstock}} \times 100\%$$

The yield of H_2, CO, CO_2 or CH_4 was calculated according to the equations showing below

$$Y_{H2}(\%) = \frac{\text{moles of } H_2\text{produced}}{4\times\text{moles of acid fed}} \times 100\%$$

$$Y_{CO/CH4/CO2}(\%) = \frac{\text{moles of } CO/CH_4/CO_2\text{produced}}{2\times\text{moles of acid fed}} \times 100\%$$

Liquid hourly space velocity (LHSV) was defined as volumetric flow rate of feed solution ((cm^3 h^{-1}) / (catalyst bed volume (cm^3)).

3. Results and discussion

3.1. Catalyst characterizations

3.1.1. TG analysis

During the impregnation of nickel species on support, nickel salts were used as the precursors of metallic nickel. The anion in the nickel salt thus needs to be removed via decomposition during calcination of the catalyst precursors. The anions in the different nickel salts might have different interaction with nickel and the support, resulting in the different decomposition temperature, which was investigated with TG analysis.

As shown in Fig. 1, anions significantly affected the decomposition of the catalyst precursors. The weight loss of $Ni(NH_2SO_3)_2/Al_2O_3$ versus temperature could be divided into three stages: the removal of moisture at ca. 100 °C, the gradual decomposition of the anion from 100 to ca. 800 °C and significant weight loss at ca. 800 °C (Fig. 1a). The EA analysis showed that the gradual loss of weight from 100 to ca. 600 °C was attributed to the release of nitrogen or the anion group, as evidenced by the sharp decrease of nitrogen content in the catalyst sample (Table 1). The TG–MS analysis indicated that the nitrogen was released in the form of NH_3 (Fig. 2a). Some sulfur in the catalyst precursors was also released in the form of SO_2, starting from 300 °C. Nevertheless, the significant release of sulfur took place at the calcination temperature of ca. 800 °C, as evidenced by the significant release of SO_2 with the TG–MS analysis (Fig. 2a).

The sulfur functionality in $NiSO_4/Al_2O_3$ sample was also released at ca. 800 °C, as evidenced by the significant weight loss (Fig. 1b). The sulfur was released in the form of SO_2, as shown in the TG-MS analysis (Fig. 2b). The elimination of the sulfur species from the catalyst with the increase of the calcination temperature from 600 to 900 °C were further confirmed with the elemental analysis, as shown in Table 1. The release of the nitrogen functionality in the NH_2SO_3– was a gradual process (Figs. 1a and 2a). It was possibly that the bonding or the interaction of nitrogen with nickel or the support was not uniform, leading to a wide span of the temperature for the release of nitrogen. In comparison, the release of sulfur took place mainly at ca. 800 °C.

The decomposition of $Ni(CH_3COO)_2/Al_2O_3$ and $Ni(NO_3)_2/Al_2O_3$ samples was also a gradual process, which, however, could be finished at around 500 °C (Fig. 1c and d). CH_3COO– is a carbon–containing functionality. It was expected that the decomposition of this functionality would produce carbon residual on surface of the catalyst. However, the EA characterization (Table 1) showed that there was no carbon residual on surface of the catalyst. It was thought that during the calcination in air the CH_3COO– was combusted or decomposed. The TG–MS result (Fig. 2c) showed that the CH_3COO– was released in the form of CO_2. The decomposition of this functionality would produce CO_2 and methyl group. The methyl group probably reacted with the oxygen in air to form CO_2 as no methane was detected.

As for $NiCl_2/Al_2O_3$, there was no sharp weight loss above 100 °C. The release of Cl element was a gradual process. The TG–MS result (Fig. 2d) showed that the Cl^- was released in the form of Cl_2. The release of the anion determined the formation of nickel oxide on surface of the carrier. This would further affect the dispersion of nickel and the interaction of nickel with alumina, which was investigated subsequently.

3.1.2. BET analysis

Surface areas of the catalyst affected dispersion of nickel species, interaction of nickel with alumina, and eventually catalytic performances. The surface area and the pore distribution of the catalysts were shown in Table 2 and Fig. 3, respectively. Alumina itself has a surface area of 257 m^2/g. The loading of nickel salts blocked some pores and led to a remarkable decrease of the specific areas for all of the catalysts. As shown in Table 2, after the impregnation of alumina with $Ni(NO_3)_2$ or $NiCl_2$, the samples had relatively higher surface areas than that impregnated with $Ni(NH_2SO_3)_2$, $NiSO_4$ or $NiCl_2$. Possibly, the nitrate and chlorine ion were relatively small and had the least influence on the specific area of the catalyst. $Ni(NH_2SO_3)_2/Al_2O_3$ had the lowest specific area. NH_2SO_3– is a relatively big anion, which, apparently, blocked the small pores of the alumina. This was evidenced by the results shown in Fig. 3a, where it can be seen that the pores in the $Ni(NH_2SO_3)_2/Al_2O_3$ catalyst after the impregnation were very limited, indicating the blockage of the pores with $Ni(NH_2SO_3)_2$. The thermal treatment of the catalyst precursors at 600 °C removed partial nitrogen element in $Ni(NH_2SO_3)_2/Al_2O_3$ catalyst (see the data in Table 1 and Fig. 2), resulting in a substantial increase of the specific area (Table 2) and the pore size (Fig. 3c).

Similar phenomena were observed for the $Ni(CH_3COO)_2/Al_2O_3$ and $Ni(NO_3)_2/Al_2O_3$ catalysts. As characterized with TG, the thermal treatment could effectively decompose the $Ni(CH_3COO)_2$ and $Ni(NO_3)_2$ salts on alumina (Fig. 1d and e), partially eliminating the blockage of the pores and resulting in an increase in surface area. Although the surface area of $NiSO_4/Al_2O_3$ catalyst also increased after the calcination at 600 °C (Table 2), the extent was very mild. From the TG characterization (Fig. 1b), it showed that the significant decomposition of the sulfate only took place at ca. 800 °C. Thus, the blockage of the pores had not been significantly improved yet. The specific area of $NiCl_2/Al_2O_3$ catalyst only increased a little bit. Cl– is relatively small, and its effect on specific area of the catalyst was also not much. Furthermore, the TG characterization (Fig. 1e) also indicated that the decomposition of $NiCl_2$ on alumina only proceeded gradually. Nevertheless, chlorine significantly affected the distribution of the pores of alumina.

After the thermal treatment at 600 °C, the abundance of the pores with the diameter above 50 Å was the highest over $NiCl_2/Al_2O_3$ catalyst (Fig. 3b). This was even more evident after the thermal treatment at 900 °C. Correspondingly, the specific area of $NiCl_2/Al_2O_3$ catalyst after the calcination at 900 °C was also the lowest (Table 2). Chlorine clearly promoted the sintering of alumina, eliminating the small pores and decreasing the specific area.

After the thermal treatment at 900 °C, the specific area of both $Ni(CH_3COO)_2/Al_2O_3$ and $Ni(NO_3)_2/Al_2O_3$ catalysts decreased from ca. 150 to ca. 75 $m^2{\cdot}g^{-1}$ (Table 2). The pore distributions for these two catalysts were also very similar. CH_3COO– or NO_3^- as the anions made no marked difference in the change of the porous structures of alumina. The specific area of $NiSO_4/Al_2O_3$ catalyst and $Ni(NH_2SO_3)_2/Al_2O_3$ catalyst also decreased after the thermal treatment at 900 °C (Table 2), extent of which was relatively mild. This was because the decomposition of the sulfate at ca. 800 °C would increase the specific area, which

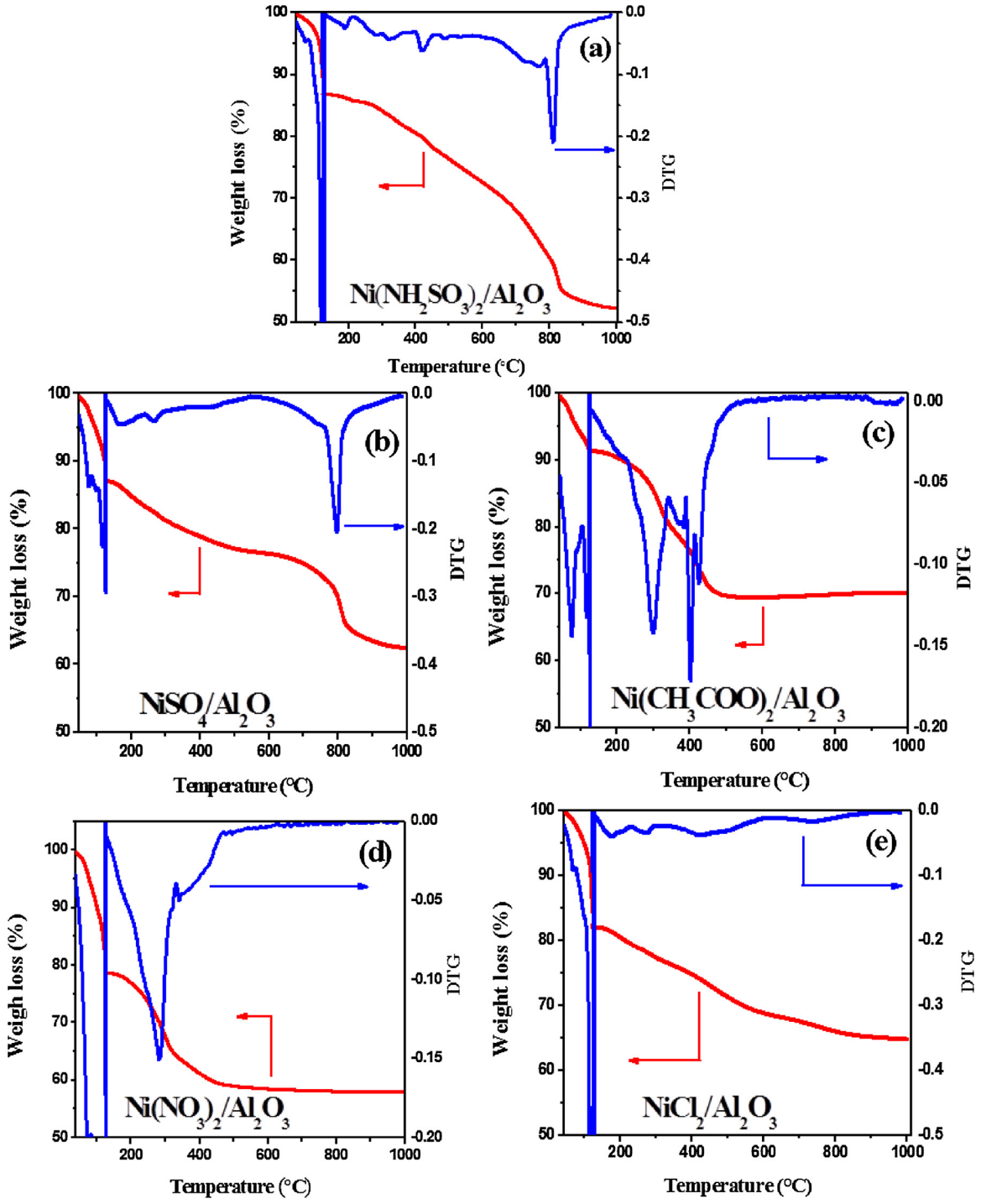

Fig. 1. TG and DTG results for the catalyst precursors without calcinations: (a): $Ni(NH_2SO_3)_2/Al_2O_3$; (b): $NiSO_4/Al_2O_3$; (c): $Ni(CH_3COO)_2/Al_2O_3$; (d): $Ni(NO_3)_2/Al_2O_3$; (e): $NiCl_2/Al_2O_3$.

could offset the decrease of the specific area induced via sintering at the high temperatures. The anions in the nickel salts affect not only the specific area of the catalyst, but also the reduction behaviors of nickel species, which was discussed in the following sections.

3.1.3. TPR characterization

Reduction profiles of the nickel catalysts after the impregnation (without calcination), after the calcination at 600 °C, and after the calcination at 900 °C were shown in Fig. 4. For the catalysts without calcination, the direct reduction of the nickel oxides in $Ni(NO_3)_2/Al_2O_3$, $Ni(CH_3COO)_2/Al_2O_3$ and $NiCl_2/Al_2O_3$ catalysts were relatively easy. The anions clearly affected the reduction behaviors of nickel species, as evidenced by the distinct locations of the reduction peaks of $Ni(NO_3)_2/Al_2O_3$ versus $NiCl_2/Al_2O_3$ (Fig. 4a and b) or the reduction profiles of $Ni(CH_3COO)_2/Al_2O_3$ (Fig. 4c). The calcination of the catalysts at 600 °C created a strong interaction between nickel species and alumina, affecting the reduction of nickel oxides. The main reduction peak of the $Ni(NO_3)_2/Al_2O_3$ catalyst shifted to ca. 800 °C. In comparison, it seemed that $CH_3COO–$ as the anion could lower the interaction of nickel with alumina, as the main reduction peak of $Ni(CH_3COO)_2/Al_2O_3$ maintained at ca. 500 °C (Fig. 4c). $NiCl_2/Al_2O_3$ also showed two main reduction peaks at 500 and 800 °C (Fig. 4b), respectively. The further

Table 1
Element analysis of Ni/Al_2O_3 catalysts prepared with different nickel precursor.

Catalysts	Element (%)			
	C	N	H	S
$Ni(NH_2SO_3)_2/Al_2O_3$ without calcinations	0.00	3.57	1.54	9.94
$Ni(NH_2SO_3)_2/Al_2O_3$ with 600 °C calcinations	0.00	1.12	1.42	9.62
$Ni(NH_2SO_3)_2/Al_2O_3$ with 900 °C calcinations	0.00	0.00	0.23	0.00
$NiSO_4/Al_2O_3$ without calcinations	0.00	0.00	0.00	7.16
$NiSO_4/Al_2O_3$ with 600 °C calcinations	0.00	0.00	0.00	7.07
$NiSO_4/Al_2O_3$ with 900 °C calcinations	0.00	0.00	0.00	0.00
$Ni(CH_3COO)_2/Al_2O_3$ without calcinations	6.06	0.00	2.94	0.00
$Ni(CH_3COO)_2/Al_2O_3$ with 600 °C calcinations	0.00	0.00	0.97	0.00
$Ni(CH_3COO)_2/Al_2O_3$ with 900 °C calcinations	0.00	0.00	0.44	0.00

increase of the calcination temperature to 900 °C further modified the reduction behaviors of nickel oxides. The reduction temperatures for the catalysts shifted to a higher region and the reduction degrees were also decreased (Table 3). As for $NiSO_4/Al_2O_3$ and $Ni(NH_2SO_3)_2/Al_2O_3$ catalysts, they showed distinct reduction behaviors (Fig. 4d and e).

The reduction peaks for $NiSO_4/Al_2O_3$ and $Ni(NH_2SO_3)_2/Al_2O_3$ catalysts after the impregnation and the calcination at 600 °C were much higher than that of others (Fig. 4d and e). The reduction degree, calculated based on the nickel oxide on alumina, was far above 100%, as shown in Table 3. In addition to nickel oxide, some other species, possibly the sulfates, must be reduced. After the calcination at 900 °C, the reduction peaks became quite small. From the TG characterization, it showed that the sulfates were decomposed at ca. 800 °C (Fig. 1a and b). Hence, the big reduction peak after the impregnation and calcination at 600 °C were possibly due to the reduction of the sulfates, which was further verified by the subsequent TPR–MS characterization (Fig. 2e and f). During the reduction of the $NiSO_4/Al_2O_3$ and $Ni(NH_2SO_3)_2/Al_2O_3$ catalysts, H_2S was formed while, during the calcination of the catalysts, SO_2 was formed (Fig. 2a and b). H_2-TPD was subsequently conducted to understand the effects of nickel salt precursors on dispersion of nickel on surface of the catalysts.

3.1.4. H_2-TPD characterization

The results for H_2-TPD of the nickel catalysts after the calcination at 600 °C and reduction at 600 °C were shown in Figure S1 in Supporting Information. The $NiSO_4/Al_2O_3$ and $Ni(NH_2SO_3)_2/Al_2O_3$ catalysts did not show any remarkable H_2-desorption peak, which was understandable. The calcination at 600 °C could not effectively decompose the sulfates, as evidenced by the slight change of sulfur content during the elemental analysis of the catalyst samples (Table 1). Although the H_2-TPR results showed that the significant reduction of both the $Ni(NH_2SO_3)_2/Al_2O_3$ and $NiSO_4/Al_2O_3$ catalysts (Fig. 4d and e), the XRD characterization showed that the nickel in the sulfates were mainly reduced to Ni_3S_2 (Fig. 5). There were no hydrogen desorption peaks during the H_2-TPD characterization over the catalysts with Ni_3S_2 as the main form of nickel, indicating that Ni_3S_2 could not effectively absorb hydrogen.

Hydrogen desorption peaks were observed for the $Ni(NO_3)_2/Al_2O_3$, $Ni(CH_3COO)_2/Al_2O_3$ and $NiCl_2/Al_2O_3$ catalysts. The hydrogen desorption profiles were quite different for the $Ni(NO_3)_2/Al_2O_3$ and $Ni(CH_3COO)_2/Al_2O_3$ catalysts, indicating the distinct interaction of hydrogen with the metallic nickel. The desorption of hydrogen initiated earlier for the $Ni(NO_3)_2/Al_2O_3$, with a main peak at ca. 479 °C and a shoulder peak at ca. 325 °C. The hydrogen desorption peaks for $Ni(CH_3COO)_2/Al_2O_3$ catalyst spanned in a wide temperature range from 450 to 750 °C. These results indicated that the metallic nickel species were not uniformly distributed on surface of alumina. The different kinetics for the desorption of hydrogen over the $Ni(NO_3)_2/Al_2O_3$ and $Ni(CH_3COO)_2/Al_2O_3$ catalysts have not been cleared yet. The dispersions of metallic nickel were summarized in Table S1 in Supporting Information. Metallic nickel had a relatively low dispersion in the catalysts investigated, which were similar to the results reported by Therdthianwong et al [44]. The catalysts were prepared via a traditional incipient wetness impregnation method with a nickel loading (on metal basis) of 20 wt%, resulting in the low nickel dispersion.

The results in Table S1 showed that the nickel dispersion over the $NiCl_2/Al_2O_3$ was the lowest, while the reduction degree of $NiCl_2/Al_2O_3$ was just a little lower than that of $Ni(NO_3)_2/Al_2O_3$ and $Ni(CH_3COO)_2/Al_2O_3$ catalysts (Table 3). Chlorine promoted the sintering of alumina support and metallic nickel, as evidenced by the lower specific area of alumina (Table 2 and Fig. 3) and the larger particle size of metallic nickel (Table 4). Nevertheless, the low dispersion of nickel in $NiCl_2/Al_2O_3$ catalyst might also relate to Kirkendall effect[45]. The melting points for $NiCl_2$ and metallic Ni were 1001 and 1455 °C, respectively. The corresponding Tammann temperature for $NiCl_2$ was relatively lower, indicating a higher diffusion rate of $NiCl_2$ than that of metallic nickel. At the elevated temperatures, the higher diffusion rate of $NiCl_2$ might lead to the formation of a core-shell structure with nickel chloride as the shell while metallic nickel as the core, as depicted in Scheme S2 in Supporting Information. This would lead to the inadequate exposure of metallic nickel species, resulting in the low dispersion of metallic nickel and the corresponding low activity for steam reforming of acetic acid.

3.1.5. NH_3-TPD

NH_3-TPD of the catalysts after calcination at 600 °C were shown in Figure S3 in Supporting Information. As the NH_3 desorption peak was very small over alumina and some catalysts, the desorption profiles of NH_3 were also depicted in Figure S3b and S3c with an enlarged view. The desorption of NH_3 across alumina carrier took place at ca. 270 and 700 °C, respectively (Figure S3b and S3c). However, the amount of the acidic sites were very small, as the intensity of the desorption peaks were several magnitudes lower than that of $Ni(NO_3)_2/Al_2O_3$ and $Ni(CH_3COO)_2/Al_2O_3$ catalysts. The desorption peaks were also very small for the $NiCl_2/Al_2O_3$, $NiSO_4/Al_2O_3$ and $Ni(NH_2SO_3)_2/Al_2O_3$ catalysts.

The TG results (Fig. 1) showed that, at the calcination temperature of 600 °C, the decomposition of $NiCl_2$ has not been completed yet while the decomposition of the sulfates have not been initiated yet. Nickel species mainly existed in the salt form. In comparison, nickel species in the $Ni(NO_3)_2/Al_2O_3$ and $Ni(CH_3COO)_2/Al_2O_3$ catalysts existed in oxide form. NiO was a basic oxide, and thus the significant amount of acidic sites in the $Ni(NO_3)_2/Al_2O_3$ and $Ni(CH_3COO)_2/Al_2O_3$ catalysts should not be originated from NiO. The acidic sites might come from some form of the interaction between NiO and alumina. $Ni(NO_3)_2/Al_2O_3$ and $Ni(CH_3COO)_2/Al_2O_3$ catalysts showed good activity for the steam reforming reactions, which might be also related to the acidic sites created by the impregnation and calcination of $Ni(NO_3)_2$ and $Ni(CH_3COO)_2$ on alumina.

The amount of acidic sites over $NiCl_2/Al_2O_3$, $NiSO_4/Al_2O_3$ and $Ni(NH_2SO_3)_2/Al_2O_3$ catalysts were relatively small. However, there were desorption peaks appeared above 700 °C over the $Ni(NH_2SO_3)_2/Al_2O_3$ and $NiSO_4/Al_2O_3$ catalysts. The desorption peaks at this high temperature might relate to the strong acidic sites created by sulfates, as SO_4^{2-} can be used to prepare the solid acid catalysts in the form of SO_4^{2-}/M_xO_y.

3.1.6. UV-vis DRS characterization

UV-vis DRS can be used to obtain some useful information on electronic effect, coordination and surface status of the chemical components in catalysts. The spectra for the catalysts with the varied precursors after impregnation and drying, after calcination at 600 °C, and after calcination at 900 °C were shown in Figure S4 in Supporting Information. The spectra in the range of 220–345 nm were attributed to the ligand charge transfer of $O^{2-} \rightarrow Ni^{2+}$ [46]. The catalyst samples before the calcination mainly have the reflection peaks located at 380–420 nm, which were the υ3 ($^3A_{2g} \rightarrow {}^3T_{1g}$ (P)) and υ2 ($^3A_{2g} \rightarrow {}^3T_{1g}$) adsorptions, originated from the d-d transitions of Ni^{2+} ions at the

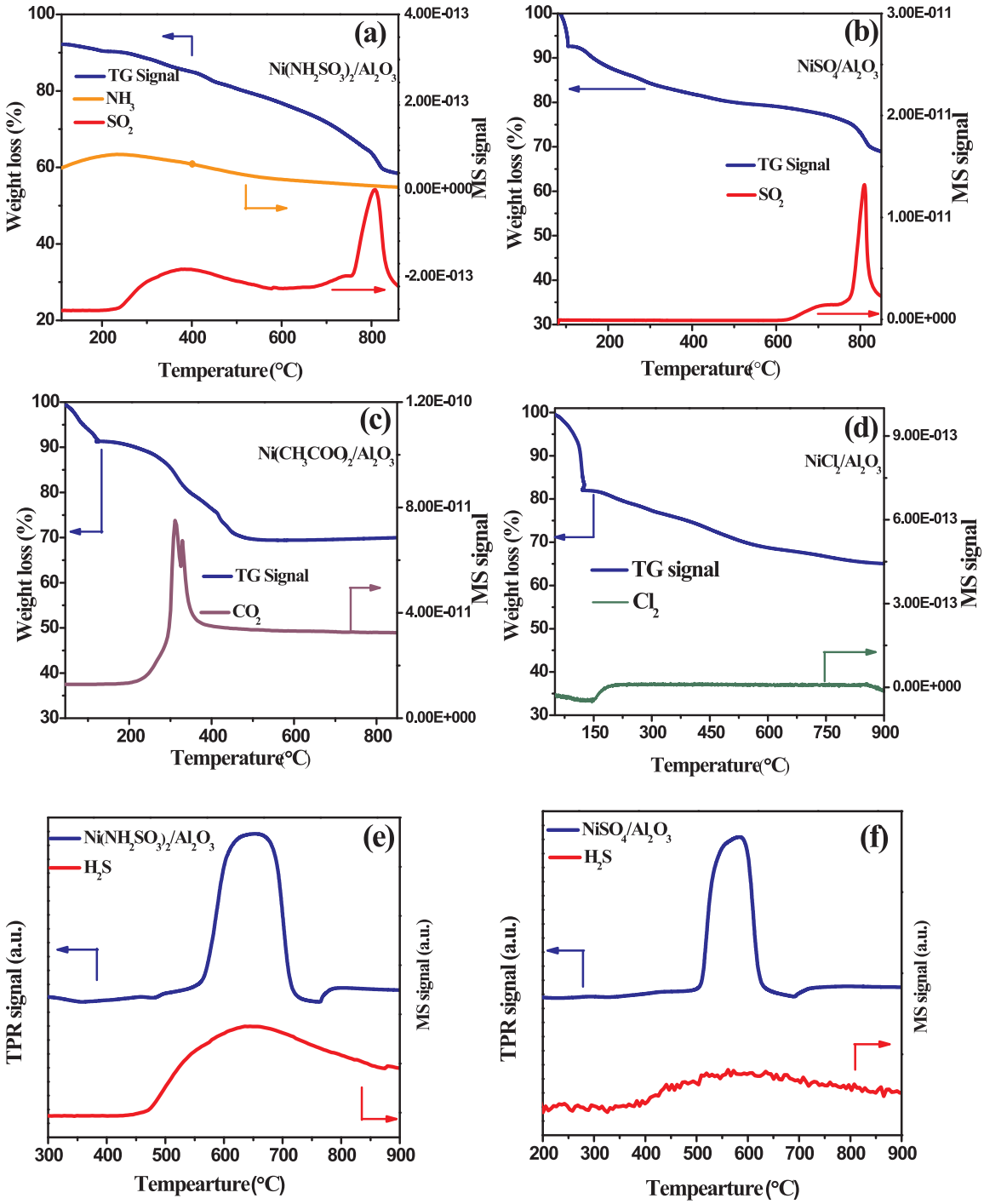

Fig. 2. TG-MS and TPR-MS results of the catalyst precursors. The TG-MS was conducted in air stream, while the TPR-MS was conducted in H_2/Ar stream: (a) TG-MS for $Ni(NH_2SO_3)_2/Al_2O_3$; (b) TG-MS for $NiSO_4/Al_2O_3$; (c) TG-MS for $Ni(CH_3COO)_2/Al_2O_3$; (d) TG-MS for $NiCl_2/Al_2O_3$; (e) TPR-MS for $Ni(NH_2SO_3)_2/Al_2O_3$; (f) TPR-MS for $NiSO_4/Al_2O_3$.

octahedral sites [47]. The coordination with the different anions led to the red or blue shift of the main peaks. After the calcination at 600 °C, the intensities of the peaks for $Ni(NO_3)_2/Al_2O_3$ and $Ni(CH_3COO)_2/Al_2O_3$ catalysts decreased significantly, while the TG characterization showed the decomposition of the nickel salts to nickel oxides. In comparison, the sulfates in $Ni(NH_2SO_3)_2/Al_2O_3$ and $NiSO_4/Al_2O_3$ did not decompose. The UV–vis DRS spectra did not change much as the coordination of nickel ions with the anions did change. In addition, there were the peaks with weak intensity appeared in the range of 550–700 nm, especially for the $NiCl_2/Al_2O_3$ catalyst, which was assigned to the ($^3T_1(F) \rightarrow {}^3T_{1g}$ (P)) ligand transitions [46]. This was the d–d electronic transition of tetrahedrally coordinated Ni^{2+} ions. The transition of the Ni^{2+} ions in the octahedral structure to the tetrahedral structures became more evident for the samples calcined at the higher temperature of 900 °C. Meanwhile, the typical adsorption band at 720 nm was also visible, which was attributed to the Ni^{2+} ions in NiO lattices. The calcination at the different temperature led to a clear change of the coordination status of the nickel species.

3.1.7. DRIFTS characterizations

DRIFTS of the catalysts were conducted to probe the transformation of the nickel salt precursors during the calcination. The adsorption

Table 2
Surface area of the catalysts after the different treatments.

Catalysts	Surface areas (m^2/g)		
	Without calcinations	Calcination at 600 °C	Calcination at 900 °C
$Ni(NO_3)_2/Al_2O_3$	139.1.0	150.2	74.0
$NiCl_2/Al_2O_3$	134.7.0	139.5	55.3
$NiSO_4/Al_2O_3$	111.0	118.2	80.3
$Ni(CH_3COO)_2/Al_2O_3$	128.1	150.8	75.9
$Ni(NH_2SO_3)_2/Al_2O_3$	10.4	74.6	65.0

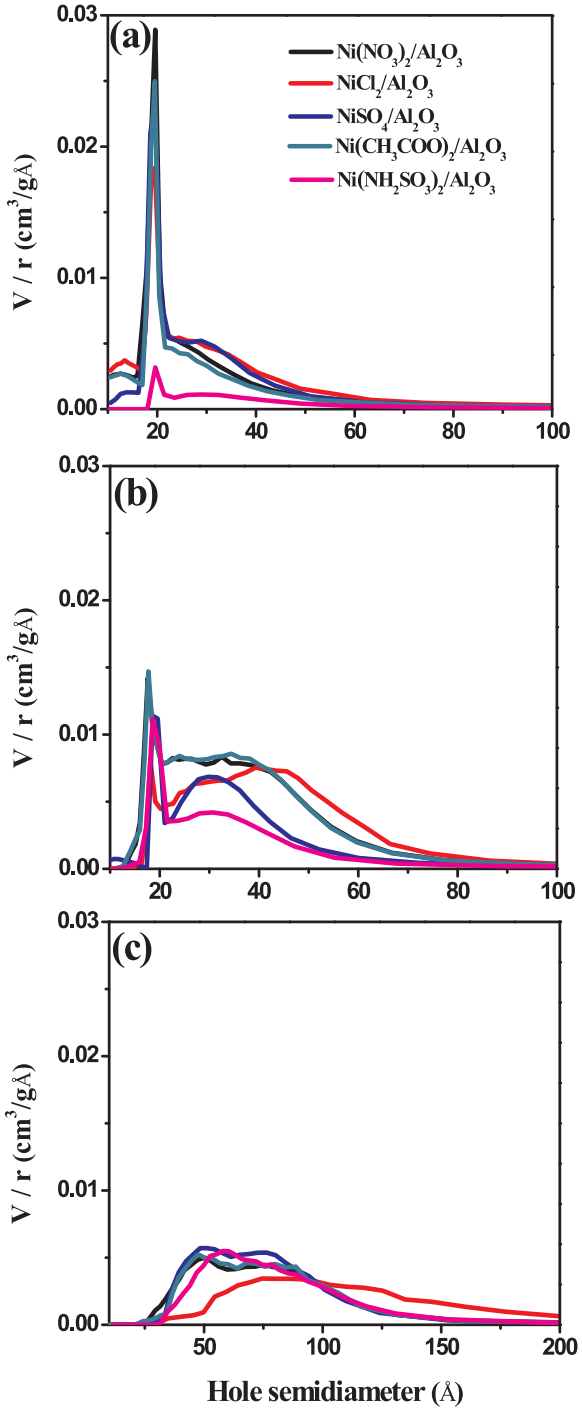

Fig. 3. The pore size distribution for (a) the catalysts without calcination; (b) the catalysts calcined at 600 °C; (c) the catalysts calcined at 900 °C.

spectra were shown in Figure S5. It is difficult to find the characteristic adsorption of the nickel salts, and thus the IR characterization of the nickel salts were also performed and the results were shown in Figure S6 (the enlarged view of the samples with relatively weak adsorption). The characteristic adsorption of $Ni(NO_3)_2$ was visible in the $Ni(NO_3)_2/Al_2O_3$ at 100 °C and the adsorption became intensified at 200 °C. There was a process of for removing the crystal water bonded and possibly a re-structure of the nickel salt on surface of the catalyst. With further increase of temperature, the peak weakened while the weak adsorption of NiO at ca. 1000 cm^{-1} appeared. Similarly, the characteristic adsorption of $Ni(CH_3COO)_2$ in $Ni(CH_3COO)_2/Al_2O_3$ weakened with the increase of the calcination temperature while the adsorption of NiO appeared. Nevertheless, the characteristic adsorption of NiO were not clear for the $NiCl_2/Al_2O_3$, $NiSO_4/Al_2O_3$ and $Ni(NH_2SO_3)_2/Al_2O_3$ catalysts.

The TG results showed that the complete decomposition of the sulfates only became significant above 800 °C. The adsorption peak for that of $NiSO_4$ at ca. 1150 cm^{-1} were obvious (Figure S6e). The adsorption of $NiCl_2$ were visible after drying the catalyst at 100 °C, while with the increasing calcination temperature the characteristic adsorption of $NiCl_2$ disappeared. The TG results (Fig. 1e) showed that the decomposition of $NiCl_2$ was a gradual process. Chlorine accelerated the sintering of alumina (Table 2 and Fig. 3). Therefore, the re-structure or the interaction of chlorine with alumina must initiated at least at 200 °C.

3.1.8. XRD characterizations

XRD characterization of the catalysts after processed at the varied conditions were shown in Fig. 5. After the impregnation and the direct reduction at 600 °C (Fig. 5a), metallic nickel and alumina were the main phases for the $Ni(NO_3)_2/Al_2O_3$ and $Ni(CH_3COO)_2/Al_2O_3$ catalysts. As for the $NiCl_2/Al_2O_3$ catalyst, the characteristic diffraction of $NiCl_2$ phase was visible (Fig. 5a). The TG result also showed that the decomposition of $NiCl_2$ was not complete at the temperature up to 600 °C (Fig. 1e). The reduction of $NiCl_2$ was relatively difficult. The XRD patterns of $NiSO_4/Al_2O_3$ and $Ni(NH_2SO_3)_2/Al_2O_3$ catalysts showed the characteristic diffractions of Ni_3S_2 phase, while diffraction of the $NiSO_4$ and the $Ni(NH_2SO_3)_2$ phases were not observed. From the TPR–MS characterization (Fig. 2), it showed that some sulfates were reduced in the form of H_2S, while from the XRD results here it showed that some sulfur reacted with nickel, forming the Ni_3S_2 compound.

After the calcination at 600 °C and the reduction at 600 °C, the diffraction patterns of the catalysts (Fig. 5b) were similar to that without the calcination (Fig. 5a). Nevertheless, the calcination generally led to the increased sizes of the nickel particle in the $Ni(NO_3)_2/Al_2O_3$ catalyst, due to the aggregation or sintering of nickel species during the heating. However, the nickel species in other catalysts behaved differently, due to the effects of the anions. The calcination of the $NiSO_4/Al_2O_3$ catalyst at 600 °C did not lead to the decomposition of $NiSO_4$. Consequently, the Ni_3S_2 phases were still observed. Similar case was observed for the $NiCl_2/Al_2O_3$ catalyst. However, after the calcination at 900 °C and the reduction at 600 °C, the Ni_3S_2 phase disappeared (Fig. 5b). The TG characterization showed that the decomposition of the sulfates took place at ca. 800 °C (Fig. 1a and b). The sulfur species were removed during the calcination process.

The calcination at 900 °C removed the sulfur species, but also led to the formation of $NiAl_2O_4$ phase (Fig. 5c). $NiAl_2O_4$ species cannot be reduced at 600 °C. However, the characteristic diffraction of $NiAl_2O_4$ species was not observed over the $Ni(CH_3COO)_2/Al_2O_3$ catalyst. $Ni(CH_3COO)_2$ as the precursor could prevent or at least suppress the solid phase reaction between nickel oxide and alumina at the high temperature, minimizing the chance for the growing of $NiAl_2O_4$ species. From the TPR characterization (Fig. 4), it did show that the calcination at 900 °C created a strong interaction between nickel and alumina, leading to the shift of the reduction temperature towards a higher region. However, the interaction did not lead to the substantial formation

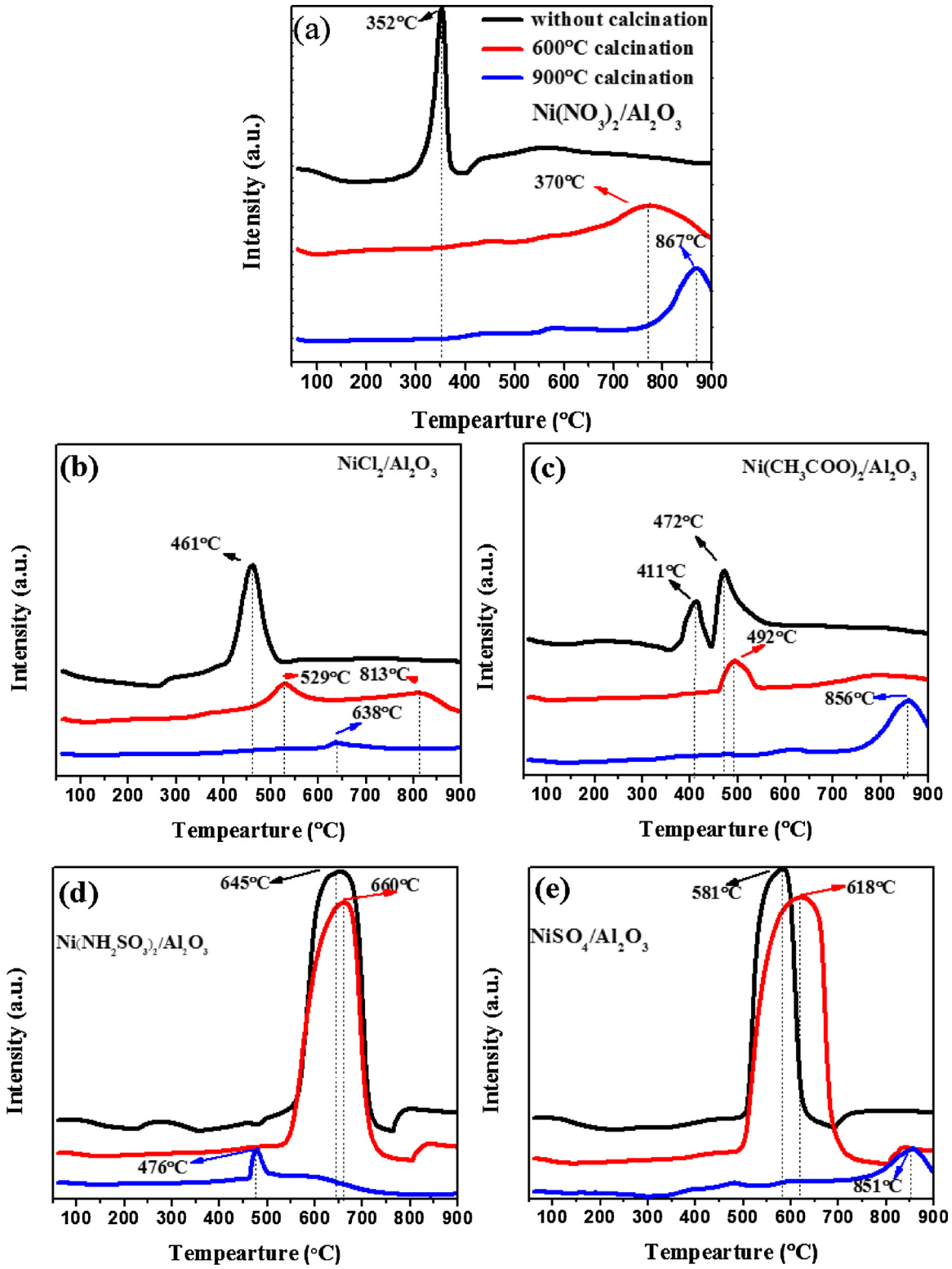

Fig. 4. TPR spectra for the catalysts prepared with the different nickel precursors: (a) $Ni(NO_3)_2/Al_2O_3$; (b) $Ni(CH_3COOH)_2/Al_2O_3$; (c) $NiCl_2/Al_2O_3$; (d) $Ni(NH_2SO_3)_2/Al_2O_3$; (e) $NiSO_4/Al_2O_3$.

of nickel–aluminum spinel.

Metallic nickel was also observed over the $NiSO_4/Al_2O_3$ and $Ni(NH_2SO_3)_2/Al_2O_3$ catalysts (Fig. 5c), suggesting that the sulfate might help to alleviate the interaction of nickel species with alumina. The increase of the reduction temperature to 800 °C could effectively reduce the formation of nickel–aluminum spinel and consequently metallic nickel became the main species across surface of the catalysts (Fig. 5d).

The above results showed that the different anions in the nickel salts substantially modified the properties of the catalysts. This would significantly impact their catalytic behaviors during steam reforming of acetic acid, which was further investigated and discussed in the following sections.

Table 3
Reduction degree of catalysts with different precursors.

Catalysts	Reduction degree (%)		
	Without calcination	600 °C calcination	900 °C calcination
$Ni(NO_3)_2/Al_2O_3$	87	69	60
$NiCl_2/Al_2O_3$	77	62	32
$NiSO_4/Al_2O_3$	341	437	63
$Ni(CH_3COO)_2/Al_2O_3$	90	69	61
$Ni(NH_2SO_3)_2/Al_2O_3$	377	394	47

Table 4
The particle sizes of Ni for the catalysts prepared with different salt precursors[a].

Catalysts	Particle size of Ni		
	Without calcination	600 °C calcination	900 °C calcination
$Ni(NO_3)_2/Al_2O_3$	11.51	14.03	–
$NiCl_2/Al_2O_3$	27.04	22.08	–
$Ni(CH_3COO)_2/Al_2O_3$	20.04	17.33	15.95
$NiSO_4/Al_2O_3$	36.12	30.20	33.42
$Ni(NH_2SO_3)_2/Al_2O_3$	27.38	25.64	28.48

[a] The nickel herein refers to the metallic nickel species in the reduced catalysts, which were calculated based on the XRD results.

3.2. Catalytic performances

The nickel catalysts, which were prepared via direct reduction but without calcination, were evaluated in steam reforming of acetic acid (Figure S7). $Ni(CH_3COO)_2/Al_2O_3$ and $Ni(NO_3)_2/Al_2O_3$ catalysts showed superior activities than the other catalysts in terms of hydrogen yield. XRD characterization (Fig. 5) showed that metallic nickel, which was active for the steam reforming reaction, was the main species in the catalysts. However, even metallic nickel was the main species in the $NiSO_4/Al_2O_3$ and $Ni(NH_2SO_3)_2/Al_2O_3$ catalysts, these two catalysts showed negligible activity for steam reforming of acetic acid. The yields of hydrogen and carbon dioxide were relatively low, while acetone, the main organic product, also could not be effectively reformed at the elevated reaction temperatures (Figure S7). After the reduction of $NiSO_4/Al_2O_3$ and $Ni(NH_2SO_3)_2/Al_2O_3$ catalysts, Ni_3S_2 were formed on surface of the catalyst. The sulfur species possibly suppressed the activity of the catalyst for the reforming reactions. On the other hand, the nickel species on the $NiSO_4/Al_2O_3$ and $Ni(NH_2SO_3)_2/Al_2O_3$ catalysts

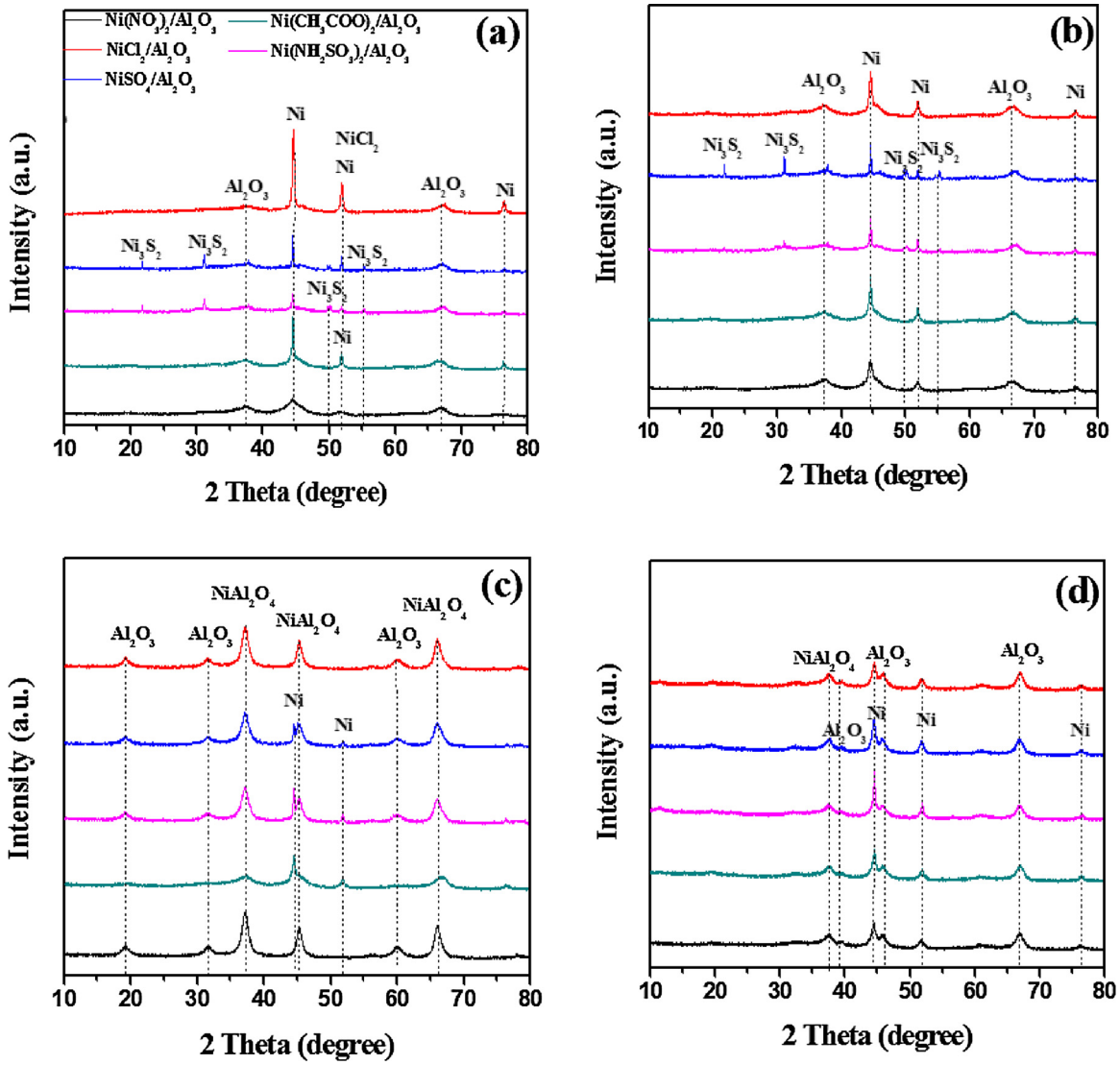

Fig. 5. XRD patterns of (a) the catalysts reduced directly at 600 °C without calcination; (b) the catalysts calcined at 600 °C and reduced at 600 °C; (c) the catalysts calcined at 900 °C and reduced at 600 °C; (d) the catalysts calcined at 900 °C and reduced at 800 °C.

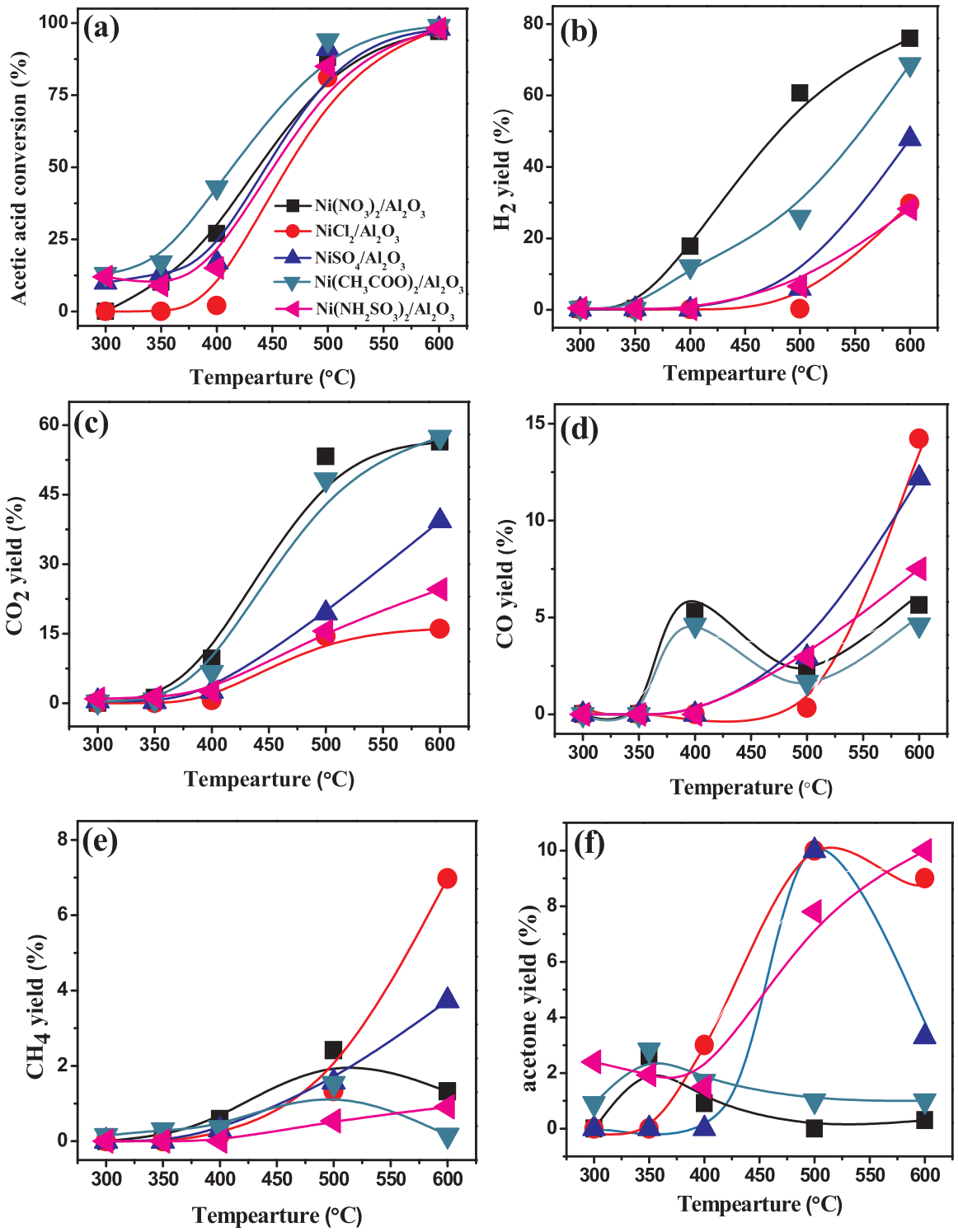

Fig. 6. Acetic acid conversion and yields of the products over the Ni/Al_2O_3 catalysts calcined at 600 °C and reduced at 600 °C. Reaction conditions: S/C = 5; LHSV = 12.7 h^{-1}; P = 1 atm.

had a large particle size (Table 4), which might have a negetive effect of the catalytic activity. $NiCl_2/Al_2O_3$ catalyst also showed low activity for the reforming reactions (Figure S7), although metallic nickel was observed in the XRD characterizations (Fig. 5). The $NiCl_2$ species were still present after reduction of the catalysts (Fig. 5a). The presence of chlorine possibly poisoned the catalysts, suppressing activity of the catalysts.

The nickel catalyst after the calcination at 600 °C (Fig. 6) showed similar activities with the catalysts without calcination (Figure S7). Ni $(CH_3COO)_2/Al_2O_3$ and $Ni(NO_3)_2/Al_2O_3$ catalysts exhibited the best activities among the ones investigated and the differences of these two catalysts in terms of catalytic behaviors were very small. The calcination at 600 °C led to a slight increase of the activity, which, however, had little impact on the catalytic activities for steam reforming of acetic acid. The other three catalysts with $NiCl_2$, $NiSO_4$ and $Ni(NH_2SO_3)_2$ as the nickel precursors still showed low activities for steam reforming of acetic acid. The presence of these heteroatoms negatively affected the catalytic activity. The calcination of the catalyst at 600 °C and the

reduction of the catalyst at 600 °C could not effectively remove these heteroatoms, as evidenced by the TG and XRD characterisations (Figs. 1 and 5). The further increase of the calcination temperature to 900 °C and the reduction temperature to 800 °C significantly impacted the catalytic behaviors.

After the calcination at 900 °C and the reduction at 600 °C (Figure S8), the catalysts except $Ni(CH_3COO)_2/Al_2O_3$ all showed negligible activities for the reforming reaction. The XRD characterization (Fig. 5) showed that at the reduction temperature of 600 °C, metallic nickel was the main phase in the $Ni(CH_3COO)_2/Al_2O_3$ catalyst (Fig. 5c). The formation of the nickel aluminate spinel was suppressed, which was the main reason for the relatively higher activity of the catalyst for acetic acid reforming. However, nickel aluminate spinel was the main phase for the $Ni(NO)_3/Al_2O_3$ catalyst, which could not be reduced at 600 °C, leading to the negligible activity of the catalyst. As discussed before, sulfates affected the formation of the nickel aluminate spinel and some metallic nickel species also could be formed even at the reduction temperature of 600 °C (Fig. 5c). However, these nickel species could not effectively catalyze the reforming reaction. It was possibly that their amount were not high enough to catalyze the reforming of acetic acid.

The reduction at 800 °C could increase activities of the catalysts to a different extent (Figure S9–S13). $Ni(CH_3COO)_2/Al_2O_3$ catalyst was active for the reforming reaction, and the reduction at the higher temperature of 800 °C improved a little of the activity. The activities of other catalysts with the exception of $NiCl_2/Al_2O_3$ were also improved as more metallic nickel species were formed via the reduction in hydrogen stream at 800 °C. Although the XRD characterization showed that metallic nickel species were presented in the reduced $NiCl_2/Al_2O_3$ catalyst (Fig. 5d), the catalyst showed almost nil activity for steam reforming of acetic acid. The presence of chlorine accelerated the sintering of the alumina carrier, leading to the most significant decrease of the surface area (Table 2). The results here clearly indicated that nickel sulfates and nickel chlorine were not the preferable nickel precursors for the preparation of nickel catalysts for steam reforming reactions. Sulfur and chlorine negatively impacted the activity of nickel for the reforming reactions and the removal of these salts required a high calcination temperature. The high calcination temperature, however, led to the sintering of alumina, leading to the decrease of the specific area and the elimination of the small pores of the support. $Ni(CH_3COO)_2$, as a precursor of metallic nickel, could suppress the formation of nickel aluminate spinel and also showed superior activity for the reforming of acetic acid.

Since the $Ni(CH_3COO)_2/Al_2O_3$ and $Ni(NO_3)_2/Al_2O_3$ catalysts showed superior activity for steam reforming of acetic acid, the catalysts with varied nickel loading (10 and 15 wt.%) were also prepared, characterized and evaluated in steam reforming of acetic acid. The BET results were shown in Table S2 and Figure S15, while the XRD results were shown in Figure S14. The conversion of acetic acid and the yields of the products were shown in Figure S16 and S17, respectively. In general, the $Ni(CH_3COO)_2/Al_2O_3$ catalysts with either nickel loading of 15 or 10 wt% showed the comparable activity for steam reforming of acetic acid. In comparison, the $Ni(NO_3)_2/Al_2O_3$ with the loading of 10 wt% showed a lower activity. The results here further confirmed the results in Fig. 6, where the $Ni(CH_3COO)_2/Al_2O_3$ catalysts showed superior capacity for steam reforming of acetic acid.

The results shown in Fig. 6 showed that the $NiCl_2/Al_2O_3$, $NiSO_4/Al_2O_3$ and $Ni(NH_2SO_3)_2/Al_2O_3$ catalysts did not show good activities for steam reforming of acetic acid. The H_2-TPD results showed that the hydrogen desorption peaks were very weak over these three catalysts (Figure S1). Chlorine and sulfur had substantial negative impact on the adsorption of H_2 on nickel sites. The H_2-TOF for the $NiCl_2/Al_2O_3$ catalyst was very low when compared with that of $Ni(NO_3)_2/Al_2O_3$ and $Ni(CH_3COO)_2/Al_2O_3$ catalysts (Table S1). Nevertheless, the yields of methane and acetone over the $NiCl_2/Al_2O_3$, $NiSO_4/Al_2O_3$ and $Ni(NH_2SO_3)_2/Al_2O_3$ catalysts were relatively higher than that over the $Ni(NO_3)_2/Al_2O_3$ and $Ni(CH_3COO)_2/Al_2O_3$ catalysts (Fig. 6). Methane and acetone were the main by-products in steam reforming of acetic acid [11].

Methane could be formed from the decomposition of acetic acid or the methanation of CO_2 with H_2 produced in steam reforming reactions [13]. Methanation reactions were generally the main reaction pathways for methane formation when the catalysts are active for steam reforming reactions [13]. This is because both methanation reactions and steam reforming reactions could be catalyzed by the same metal such as nickel [13]. At the higher reaction temperature, the methanation reaction was suppressed due to the reaction equilibrium, and meanwhile the steam reforming of methane also initiated, leading to the decreased production of methane, which was the case for $Ni(NO_3)_2/Al_2O_3$ and $Ni(CH_3COO)_2/Al_2O_3$ catalysts. Decomposition of acetic acid would become the main reaction route for the formation of methane at the elevated temperatures when the catalysts were not active for steam reforming reactions. Herein, this was the case for the $NiCl_2/Al_2O_3$, $NiSO_4/Al_2O_3$ and $Ni(NH_2SO_3)_2/Al_2O_3$ catalysts, which showed the high selectivity for methane production at the elevated temperature.

Acetone was mainly formed from ketonization of acetic acid, which was generally produced when the catalyst was not active for steam reforming of acetic acid. This is because ketonization of acetic acid and steam reforming of acetic acid were competitive reactions. Over $Ni(NO_3)_2/Al_2O_3$ and $Ni(CH_3COO)_2/Al_2O_3$ catalysts, the ketonization of acetic acid proceeded at the low temperatures (Fig. 6f), formation of which was soon suppressed due to the dominance of steam reforming reactions. Furthermore, with the acceleration of steam reforming reactions, the acetone, which was produced from the ketonization of acetic acid, could even be reformed with steam, resulting in its decreased production at the elevated temperature. Nevertheless, for the $NiCl_2/Al_2O_3$, $NiSO_4/Al_2O_3$ and $Ni(NH_2SO_3)_2/Al_2O_3$ catalysts, their activities for steam reforming were relatively low, and thus the unconverted acetic acid would have more chance to be converted to acetone via the ketonization reaction. The acetone produced also could not be effectively reformed, leading to the presence of the significant amount of acetone in the products.

Both $Ni(NO_3)_2/Al_2O_3$ and $Ni(CH_3COO)_2/Al_2O_3$ catalysts were active for steam reforming of acetic acid. The two catalysts generally had the comparable activity for the reforming reactions. The distribution of the products were also similar. For example, the production of methane reached the maximum at 500 °C, and the formation of acetone reached the maximum at 350 °C for both the catalysts. The reaction pathways for the formation of methane and acetone over these two catalysts were largely similar. The $Ni(CH_3COO)_2/Al_2O_3$ and $Ni(NO_3)_2/Al_2O_3$ catalysts have almost identical surface areas and very similar pore volumes and mean pore radiuses (Table S1 in Supporting Information). Nevertheless, the dispersion of nickel particle in the $Ni(CH_3COO)_2/Al_2O_3$ catalyst was relatively higher than that over $Ni(NO_3)_2/Al_2O_3$ catalyst. The different dispersion of metallic nickel originated from the distinct interaction of nickel with alumina, which further affected the desorption of H_2. $CH_3COO–$ is bigger than $NO_3–$, which might help to promote the dispersion of nickel species on alumina. Nevertheless, with $Ni(CH_3COO)_2$ or $Ni(NO_3)_2$ as the precursor did impact the interaction of nickel species with alumina. Calcination temperature impacted the interaction of nickel with alumina. The two catalysts produced without calcination and with direct reduction showed comparable activity for steam reforming of acetic acid (Figure S7). Nevertheless, the calcination at 900 °C induced the strong interaction between nickel and alumina, forming the nickel-alumina spinel. After the reduction at 600 °C in hydrogen stream, the $Ni(NO_3)_2/Al_2O_3$ catalyst showed almost no activity for steam reforming of acetic acid, while the $Ni(CH_3COO)_2/Al_2O_3$ catalyst showed a much higher activity (Figure S8). $Ni(CH_3COO)_2$ as the precursor could alleviate the interaction of nickel with alumina. With the higher reduction temperature of 800 °C, the nickel in $Ni(NO_3)_2/Al_2O_3$ catalyst could also be reduced, and the catalyst showed comparable activity with the $Ni(CH_3COO)_2/Al_2O_3$ catalyst (Figure S9). Although the $Ni(NO_3)_2/Al_2O_3$ and $Ni(CH_3COO)_2/Al_2O_3$ catalysts

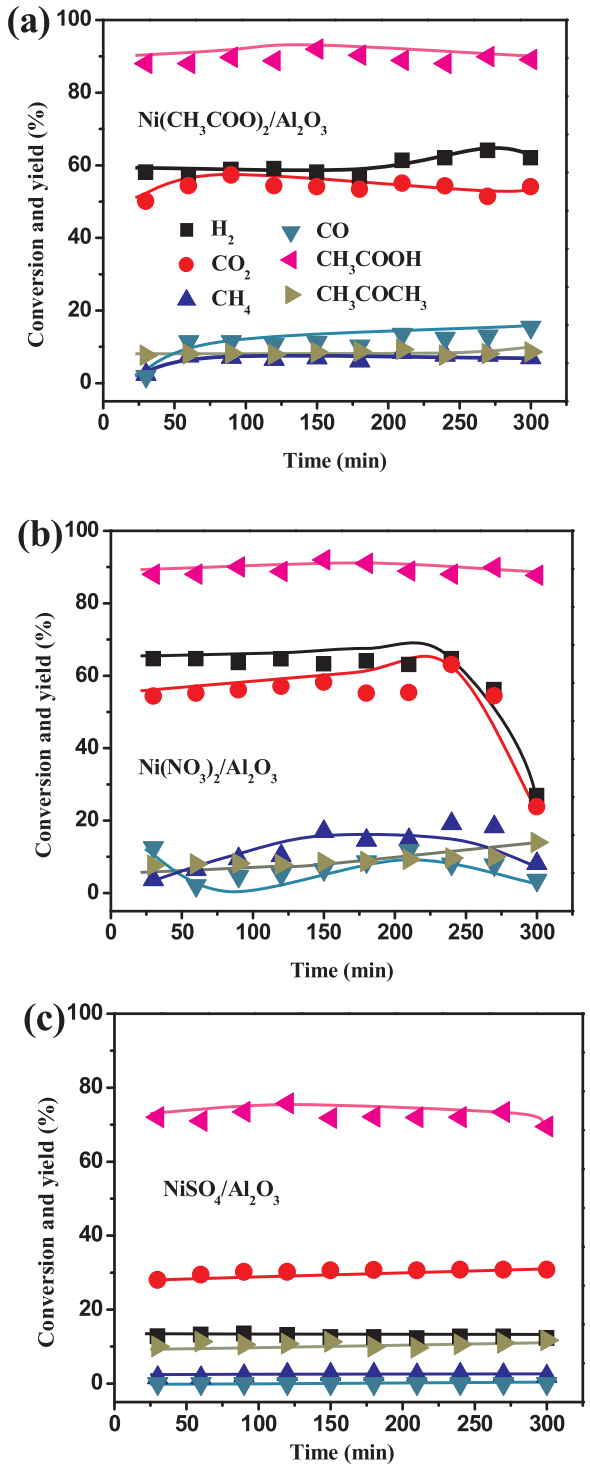

Fig. 7. Stability tests of the catalysts in steam reforming of acetic acid. (a) Ni $(CH_3COO)_2/Al_2O_3$; (b) $Ni(NO_3)_2/Al_2O_3$; (c) $NiSO_4/Al_2O_3$. Reaction conditions: S/C = 1.5; LHSV = 12.7 h^{-1}; P = 1 atm.

showed the comparable activity for steam reforming of acetic acid, they did not show the same reaction behaviors in the stability tests, which were further investigated.

3.3. Stability of the catalysts and the tendency towards coke deposition

Stability of the nickel catalysts versus reaction time was further investigated at 500 °C with an S/C of 1.5. As shown in Fig. 7, the activity of the $Ni(CH_3COO)_2/Al_2O_3$ catalyst was relatively stable during the whole time–on–stream investigated. In comparison, the activity of $Ni(NO_3)_2/Al_2O_3$ declined significantly at the end of the test. The $NiSO_4/Al_2O_3$ catalyst, which was calcined at 900 °C and reduced at 800 °C, showed a negligible activity for the steam reforming of acetic acid. Coke formation could be an important factor affecting stability of the catalysts in the reforming reaction, which was further investigated with TG characterization.

The TG results were shown in Fig. 8. The weight loss of the spent Ni $(NO_3)_2/Al_2O_3$ catalyst was obviously higher than the weight loss of the spent $Ni(CH_3COO)_2/Al_2O_3$ catalyst. More coke formed on $Ni(NO_3)_2/Al_2O_3$, which was probably the main reason for the deactivation of the $Ni(NO_3)_2/Al_2O_3$ catalyst during the stability tests (Fig. 7). The $NiSO_4/Al_2O_3$ showed a negligible activity during the steam reforming of acetic acid. Thus, the coke formation over $NiSO_4/Al_2O_3$ was not serious (Fig. 8e). The cleavage of the C—C bond of acetic acid generally involves the formation of the CH_x species, which is an important catalyst precursor for the formation of coke. However, the conversion of acetic acid over the $NiSO_4/Al_2O_3$ was low, which reduced the chance for the formation of coke. The weight loss of the $Ni(NO_3)_2/Al_2O_3$ and Ni $(CH_3COO)_2/Al_2O_3$ catalysts could be divided into several stages by the DTG result, which was probably due to the formation of the different kinds of coke on surface of the catalysts. This was further analyzed with TPO-MS characterization.

The TPO-MS results were shown in Fig. 8, where the oxygen consumption peaks distributed in a wide range. For the spent $Ni(NO_3)_2/Al_2O_3$, the oxygen consumption peak located at ca. 688 and ca. 743 °C (Fig. 8d), respectively, which probably represented two types of coke species with different structures. For the spent $Ni(CH_3COO)_2/Al_2O_3$, only a major peak at ca. 632 °C was visible (Fig. 7b). In addition, during the oxidation of the coke species, CO was simultaneously generated with the formation of CO_2. The CO formation might be due to the incomplete oxidation of the coke species. The abundance or the tendencies for the formation of CO and CO_2 were also different over the different catalyst. The structure of the coke was probably different, which was further investigated by TEM and Raman characterization.

The TEM characterization for measuring the morphology of the coke formed on the $Ni(NO_3)_2/Al_2O_3$ and $Ni(CH_3COO)_2/Al_2O_3$ catalysts were shown in Fig. 9. Fibrous coke and amorphous coke were formed on surface of both of the catalysts. It was reported that the fibrous coke had less effect on catalytic activity while the amorphous coke blocked nickel sites and negatively affected the catalytic activity [48]. The TPO results herein clearly showed that the coke species were not uniformly formed on the catalyst. In addition, the diameter of the fibrous coke was around ca. 3 nm over the $Ni(CH_3COO)_2/Al_2O_3$ catalyst (Fig. 8a) while the diameter of the fibrous coke over the $Ni(NO_3)_2/Al_2O_3$ catalyst was around 4–5 nm (Fig. 8b). This was probably due to the higher amount of coke formed over the $Ni(NO_3)_2/Al_2O_3$ catalyst and the fibrous coke species could grow bigger.

The EDS characterizations of the spent catalysts after the stability tests were shown in Figure S18, S19 and S20 for the $NiSO_4/Al_2O_3$, Ni $(CH_3COO)_2/Al_2O_3$ and $Ni(NO_3)_2/Al_2O_3$, respectively. The C species could be found on surface of the catalysts. Nevertheless, the density of the C species were different, which followed the order: $NiSO_4/Al_2O_3$ < $Ni(CH_3COO)_2/Al_2O_3$ < $Ni(NO_3)_2/Al_2O_3$. The results were in line with the TG characterization shown in Fig. 8, where the coke formation was the most serious over the spent $Ni(NO_3)_2/Al_2O_3$ catalyst, and followed by the spent $Ni(CH_3COO)_2/Al_2O_3$ and $NiSO_4/Al_2O_3$ catalysts. The coke formation over the $NiSO_4/Al_2O_3$ was not serious, which was related to the low activity of the catalyst for steam reforming of acetic acid. $Ni(CH_3COO)_2/Al_2O_3$ catalyst showed a higher resistivity towards coke formation than $Ni(NO_3)_2/Al_2O_3$ catalyst, which might be due to the higher metallic nickel dispersion over the $Ni(CH_3COO)_2/Al_2O_3$ catalyst. The internal structure of the coke species were further investigated with Raman analysis to further understand the different structures of the coke.

The Raman spectra for the spent catalyst were shown in Fig. 9e. The

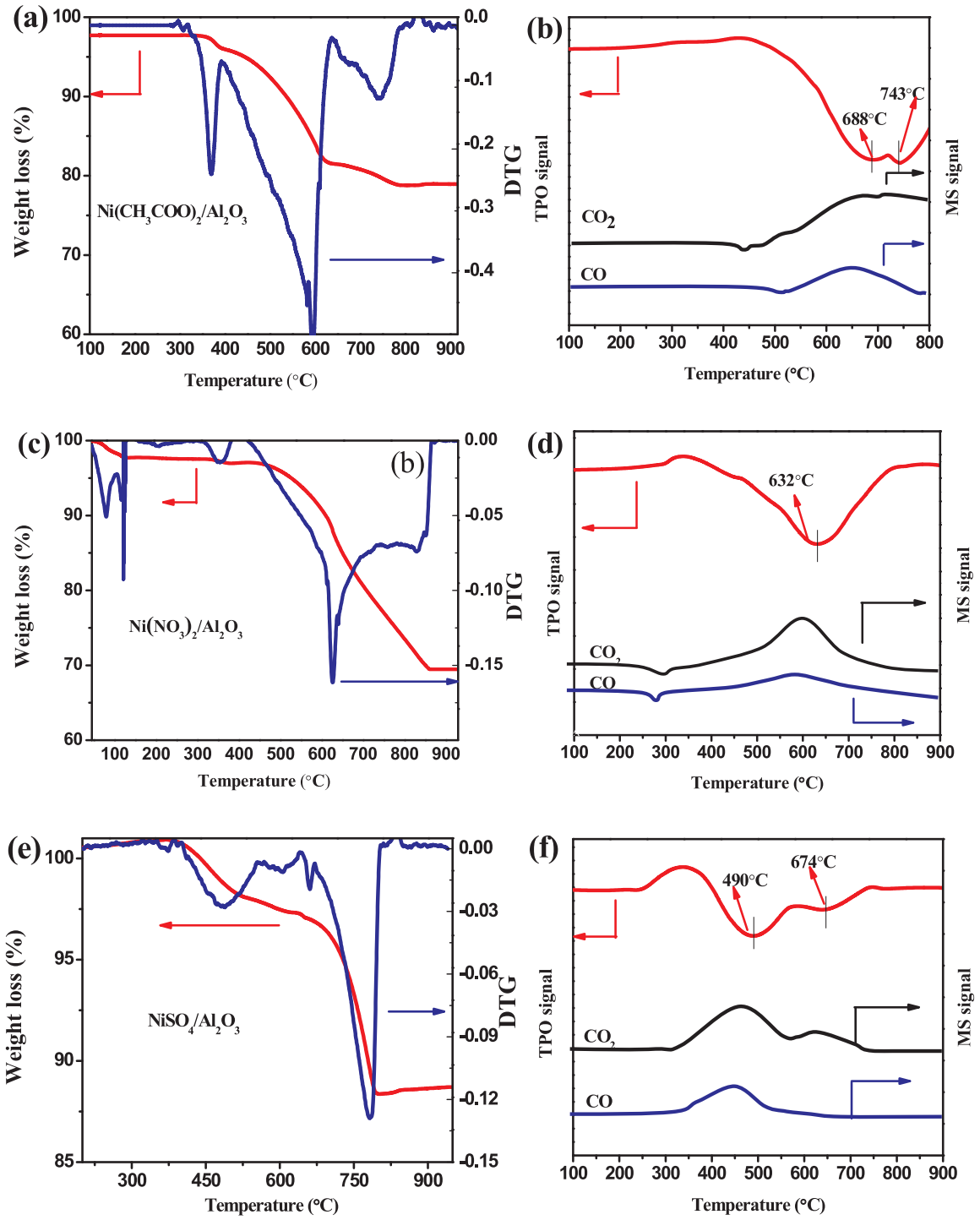

Fig. 8. TG and TPO-MS curves of the catalysts after the stability test. The TG characterizations were conducted in air stream, while the TPO-MS was conducted in O_2/He stream. (a) TG-MS of $Ni(CH_3COO)_2/Al_2O_3$; (b) TPO-MS of $Ni(CH_3COO)_2/Al_2O_3$; (c) TG-MS of $Ni(NO_3)_2/Al_2O_3$; (d) TPO-MS of $Ni(NO_3)_2/Al_2O_3$; (e) TG-MS of $NiSO_4/Al_2O_3$; (f) TPO-MS of $NiSO_4/Al_2O_3$.

first peak centered at ca. 1350cm^{-1}, which represented the large aromatic ring structures (D band). The second peak, which located at ca. 1575cm^{-1}, represented the small aromatic ring structures (G band). The coke in the spent catalysts all contained the large and the small aromatic ring structures. The ratios of the D band to the G band were similar for the $Ni(NO_3)_2/Al_2O_3$ and $Ni(CH_3COO)_2/Al_2O_3$ catalysts. The formation of the large or the small aromatic ring system did not have a special preference over these two catalysts. However, the ratio of D band to G band in the $NiSO_4/Al_2O_3$ catalyst was smaller, indicating that more smaller aromatic ring system were formed on this catalysts. In addition, the total Raman area was much higher over $NiSO_4/Al_2O_3$ catalyst than over the other two catalysts, indicating that the abundance of the oxygen–containing functionalities was much higher in the coke formed over this catalyst. Functionality of the coke over the catalysts was further analyzed with DRIFTS characterization.

The results of DRIFTS characterization showed that the coke contained the C═C and C—O bonds (Fig. 10). The coke might also contain the hydroxyl group, as the hydroxyl group might also be the ones attached on the surface of alumina. The abundance of the C—O bond at ca. 1000 cm^{-1} over the $NiSO_4/Al_2O_3$ catalyst was much higher than that

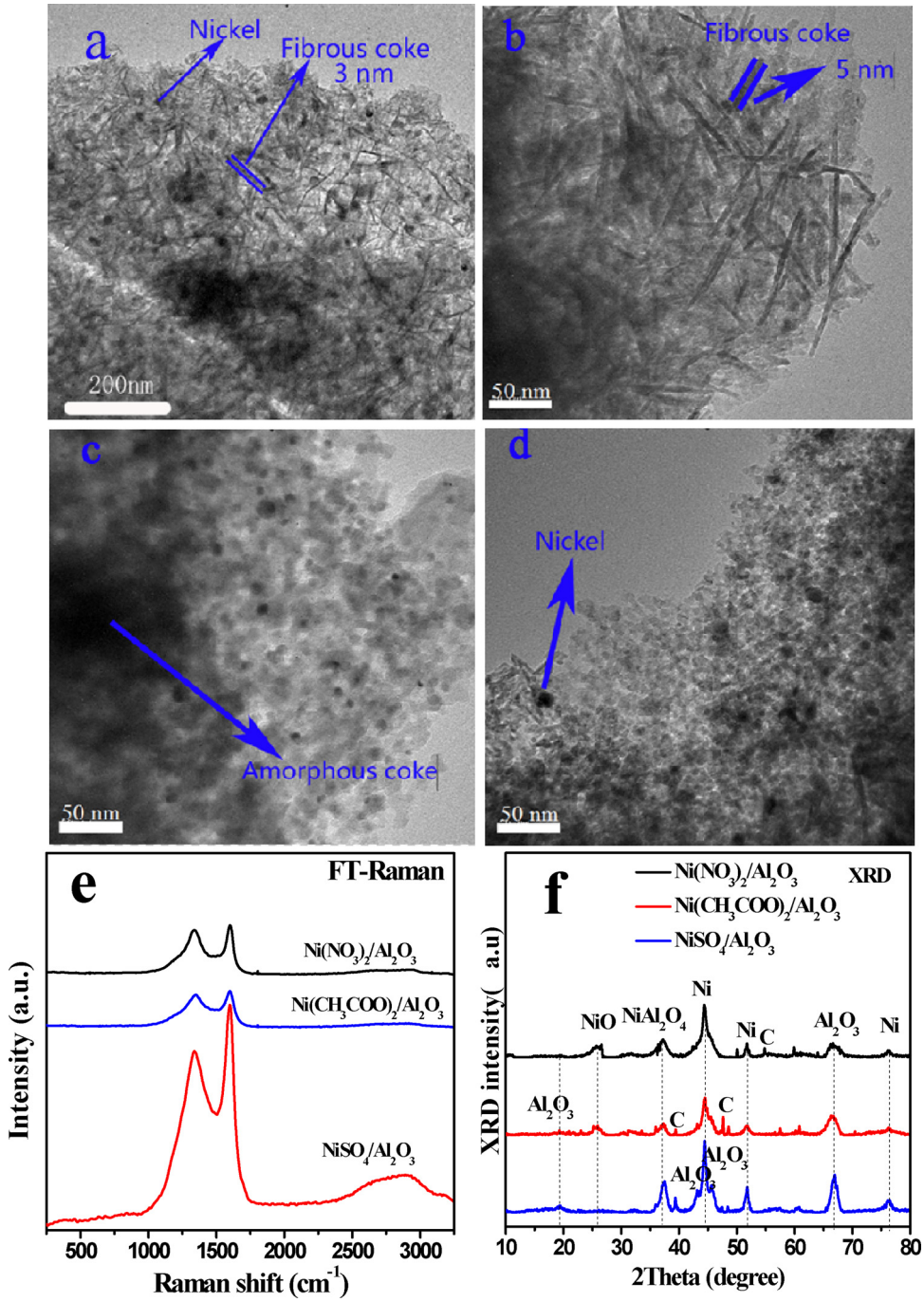

Fig. 9. TEM images, FT-Raman and XRD results of the catalysts after stability tests. (a) and (c): $Ni(CH_3COO)_2/Al_2O_3$; (b): $Ni(NO_3)_2/Al_2O_3$; (d):$NiSO_4/Al_2O_3$; (e): FT-Raman curves of the catalysts; (f): XRD curves of the catalysts.

over the other two catalysts, which was in line with the Raman results, where high abundance of oxygen–containing functionalities existed over this catalyst (Fig. 10a). XRD characterization of the spent catalysts were also conducted, as shown in Fig. 9f. Metallic nickel and alumina were the main species on the catalysts. Nevertheless, the characteristic diffraction of coke species was also visible over the three catalysts investigated. The crystal structures of the carbon species were different over the $Ni(NO_3)_2/Al_2O_3$ than over the other catalysts, indicating the different mechanism for formation of the coke, which needs further investigation.

FT-IR and TG-MS analysis of the spent catalysts were further conducted to explore properties of the coke formed in the stability tests. The FT–IR characterization (Figure S22) showed that the coke contained C═O, C═C and aromatic ring structures. The Ar-H absorption over the $Ni(NO_3)_2/Al_2O_3$ catalyst was much stronger than the other two catalysts. The structures of the coke were different over the different catalysts, which was further proved via the TG-MS characterization in inert atmosphere (Figure S23). The weight loss for the Ni $(CH_3COO)_2/Al_2O_3$ catalyst was much higher than that of the $Ni(NO_3)_2/Al_2O_3$, indicating that the coke over the $Ni(NO_3)_2/Al_2O_3$ was thermally more stable. In addition, over the $Ni(NO_3)_2/Al_2O_3$ catalyst, the H_2 peak was observed above 600 °C, indicating that the dehydrogenation reaction took place. Meanwhile, the appearance of CH_4 peak indicated that the coke species possibly contained methyl functionality. The formation of CO and CO_2 at ca. 800 °C suggested that the coke might contain carbonyl and carboxylic groups, which were in line with the FT-IR

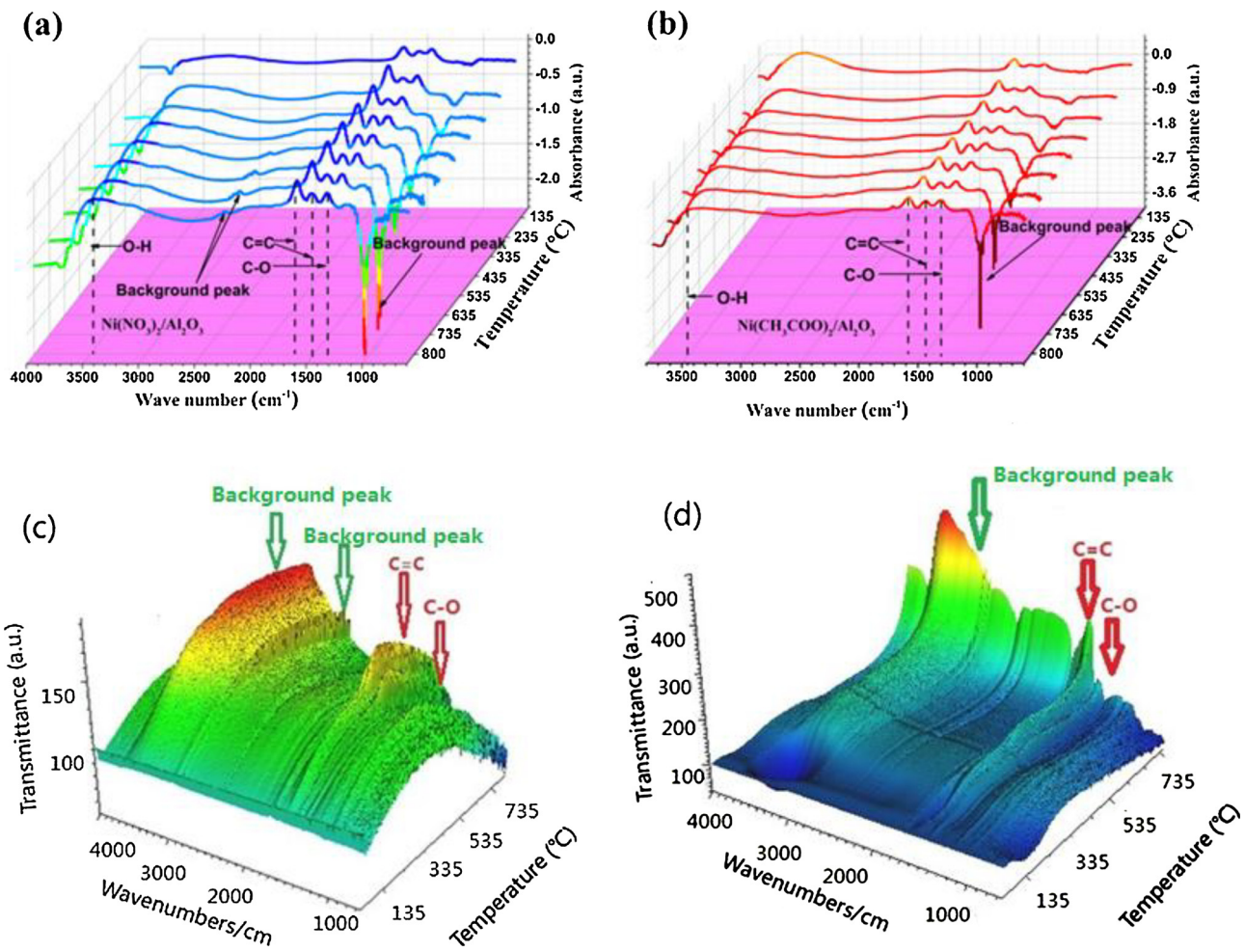

Fig. 10. DRIFTS curves of the catalysts after the stability tests. The characterizations were conducted under the condition of vacuum. (a) and (c): $Ni(NO_3)_2/Al_2O_3$; (b) and (d): $Ni(CH_3COO)_2/Al_2O_3$.

result (Figure S22). Over the $Ni(CH_3COO)_2/Al_2O_3$ catalyst, the formation of CO_2 versus temperature peaked at three temperatures, and no significant CO releasing peak was observed at the high reaction temperature, which clearly indicated the distinct structure of the coke with that over $Ni(NO_3)_2/Al_2O_3$ catalyst. The profiles for releasing the gaseous products over $NiSO_4/Al_2O_3$ catalyst was different from the other two catalysts, inducing from the different coke species formed.

4. Conclusions

In summary, the type of anion in the nickel salts significantly affect the properties and catalytic behaviors of the Ni/Al_2O_3 catalysts. $NiSO_4/Al_2O_3$ and $Ni(NH_2SO_3)_2/Al_2O_3$ calcined and reduced at 600 °C did not show good reforming activity, as at this temperature the sulfates were reduced and reacted with metallic nickel to form of Ni_3S_2. Ni_3S_2 was not the active species for steam reforming of acetic acid. The effective decomposition of the sulfates occurred at ca. 800 °C. Nevertheless, at this temperature the sintering of the support also took place. The size of the NH_2SO_3– anion is relatively big, which could block some pores of the alumina during impregnation of the salt. The sulfur element in the catalysts were released in the form of SO_2 during the calcination in air or in the form of H_2S during the reduction with hydrogen. $NiCl_2/Al_2O_3$ showed a negligible activity for steam reforming of acetic acid. The chlorine salt was difficult to decompose, which poisoned the nickel species. More importantly, chlorine interacted with alumina, accelerating the sintering of alumina and leading to a reduced specific area and an increased pore diameter.

$Ni(NO_3)_2/Al_2O_3$ and $Ni(CH_3COO)_2/Al_2O_3$ catalysts showed good while similar activity for steam reforming of acetic acid. The CH_3COO– decomposed in the form of CO_2 during the calcination in air. Both NO_3– and CH_3COO– as the anions did not impose negative effects on activity of the catalyst. However, $Ni(CH_3COO)_2/Al_2O_3$ catalyst was more stable than the $Ni(NO_3)_2/Al_2O_3$ catalyst and has a higher resistivity towards coke formation. CH_3COO– as the anion could effectively suppress the formation of nickel–alumina spinal. Such an effect was not observed over the catalysts prepared with the other nickel precursors investigated. In addition, the coke formed over the $Ni(NO_3)_2/Al_2O_3$ and $Ni(CH_3COO)_2/Al_2O_3$ catalysts had the large and small aromatic ring structures with the morphology of both amorphous and fibrous forms. In short, among the nickel precursors investigated, $Ni(CH_3COO)_2$ was more suitable as the precursor for Ni/Al_2O_3 catalyst as CH_3COO– can decompose completely in the form of CO_2 and the catalysts prepared showed a good activity for steam reforming of acetic acid and superior stability among the catalysts investigated. Metal precursors have significant effects on the properties and catalytic behaviors of the nickel-based catalysts, which should be taken into consideration in preparation of not only nickel-based catalysts but also other heterogeneous catalysts.

Acknowledgements

This work was supported by the Strategic International Scientific and Technological Innovation Cooperation Special Funds of National Key R&D Program of China (No. 2016YFE0204000), the Program for

Taishan Scholars of Shandong Province Government, the Recruitment Program of Global Young Experts (Thousand Youth Talents Plan), Natural Science Fund of Shandong Province (ZR2017BB002) and the Foundation of State Key Laboratory of Coal Combustion.

Appendix A. Supplementary data

Supplementary material related to this article can be found, in the online version, at doi:https://doi.org/10.1016/j.apcatb.2018.06.020.

References

[1] D. Wang, D. Montané, E. Chornet, Appl. Catal. A: Gen. 143 (1996) 245–270.
[2] C. Rioche, S. Kulkarni, F.C. Meunier, J.P. Breen, R. Burch, Appl. Catal. B: Environ. 61 (2005) 130–139.
[3] J. Pu, K. Nishikado, N. Wang, T.T. Nguyen, T. Maki, E.W. Qian, Appl. Catal. B: Environ. 224 (2018) 69–79.
[4] J. Chen, M. Tamura, Y. Nakagawa, K. Okumura, K. Tomishige, Appl. Catal. B: EnViron. 179 (2015) 412–421.
[5] F. Che, S. Ha, J.-S. McEwen, Appl. Catal. B: Environ. 195 (2016) 77–89.
[6] A.H. Braga, E.R. Sodré, J.B.O. Santos, C.M. de Paula Marques, J.M.C. Bueno, Appl. Catal. B: Environ. 195 (2016) 16–28.
[7] Z. Zhang, X. Hu, J. Li, G. Gao, D. Dong, R. Westerhof, S. Hu, J. Xiang, Y. Wang Fuel. 217 (2018) 389–403.
[8] L. Zhang, G. Hu, S. Hu, J. Xiang, X. Hu, X. Hu, Y. Wang, D. Geng, Sustain. Energy Fuels (2018), http://dx.doi.org/10.1039/C8SE00006A.
[9] Z.-Y. Du, Y.-X. Ran, Y.-P. Guo, J. Feng, W.-Y. Li, Appl. Surf. Sci. 419 (2017) 114–125.
[10] Y.-X. Ran, Z.-Y. Du, Y.-P. Guo, J. Feng, W.-Y. Li, Appl. Surf. Sci. 400 (2017) 97–109.
[11] A.C. Basagiannis, X.E. Verykios, Int. J. Hydrogen Energy 32 (2007) 3343–3355.
[12] J. Li, P. Jia, X. Hu, D. Dong, G. Gao, D. Geng, J. Xiang, Y. Wang, S. Hu, Mol. Catal. 450 (2018) 1–3.
[13] V. Palma, C. Ruocco, E. Meloni, A. Ricca, J. Clean. Prod. 166 (2017) 263–272.
[14] X. Hu, G. Lu, J. Mol. Catal. A: Chem. 261 (2007) 43–48.
[15] O.A. Omoniyi, V. Dupont, Appl. Catal. B: Environ. 226 (2018) 258–268.
[16] F.G.E. Nogueira, P.G.M. Assaf, H.W.P. Carvalho, E.M. Assaf, Appl. Catal. B: Environ. 160–161 (2014) 188–199.
[17] T.M.C. Hoang, B. Geerdink, J.M. Sturm, L. Lefferts, K. Seshan, Appl. Catal. B: Environ. 163 (2015) 74–82.
[18] F. Bossola, C. Evangelisti, M. Allieta, R. Psaro, S. Recchia, V. Dal Santo, Appl. Catal. B: Environ. 181 (2016) 599–611.
[19] R.M. Navarro, R. Guil-Lopez, A.A. Ismail, S.A. Al-Sayari, J.L.G. Fierro, Catal. Today. 242 (2015) 60–70.
[20] M.V. Gil, J. Fermoso, C. Pevida, D. Chen, F. Rubiera, Appl. Catal. B: Environ. 184 (2016) 64–76.
[21] F. Cheng, V. Dupont, Int. J. Hydrogen Energy 38 (2013) 15160–15172.
[22] G. Garbarino, A. Lagazzo, P. Riani, G. Busca, Appl. Catal. B: Environ. 129 (2013) 460–472.
[23] B. Valle, B. Aramburu, A. Remiro, J. Bilbao, A.G. Gayubo, Appl. Catal. B: Environ. 147 (2014) 402–410.
[24] G. Garbarino, E. Finocchio, A. Lagazzo, I. Valsamakis, P. Riani, V.S. Escribano, G. Busca, Appl. Catal. B: Environ. 147 (2014) 813–826.
[25] M. El Doukkali, A. Iriondo, P.L. Arias, J. Requies, I. Gandarías, L. Jalowiecki-Duhamel, F. Dumeignil, Appl. Catal. B: Environ. 125 (2012) 516–529.
[26] S. Natesakhawat, R.B. Watson, X. Wang, U.S. Ozkan, J. Catal. 234 (2005) 496–508.
[27] J. Zhang, H. Xu, X. Jin, Q. Ge, W. Li, Appl. Catal. A: Gene. 290 (2005) 87–96.
[28] H.-S. Roh, K.-W. Jun, W.-S. Dong, J.-S. Chang, S.-E. Park, Y.-I. Joe, J. Mol. Catal. A: Chem. 181 (2002) 137–142.
[29] H. Yang, S. Song, R. Rao, X. Wang, Q. Yu, A. Zhang, J. Mol. Catal. A: Chem. 323 (2010) 33–39.
[30] J. Yoo, Y. Bang, S.J. Han, T.H. Kang, J. Lee, I.K. Song, J. Mol. Catal. A: Chem. 380 (2013) 28–33.
[31] Z. Li, X. Hu, L. Zhang, G. Lu, J. Mol. Catal. A: Chem. 355 (2012) 123–133.
[32] K.K. Pant, P. Mohanty, S. Agarwal, A.K. Dalai, Catal. Today. 207 (2013) 36–43.
[33] B. Abdullah, N.A. Abd Ghani, D.-V.N. Vo, J. Clean. Prod. 162 (2017) 170–185.
[34] L. Zhang, X. Wang, B. Tan, U.S. Ozkan, J. Mol. Catal. A: Chem. 297 (2009) 26–34.
[35] S. Goicoechea, E. Kraleva, S. Sokolov, M. Schneider, M.-M. Pohl, N. Kockmann, H. Ehrich, Appl. Catal. A: Gene. 514 (2016) 182–191.
[36] P. Kim, H. Kim, J.B. Joo, W. Kim, I.K. Song, J. Yi, J. Mol. Catal. A: Chem. 256 (2006) 178–183.
[37] J.T. Richardson, R.M. Scates, M.V. Twigg, Appl. Catal. A: Gene. 267 (2004) 35–46.
[38] M.C. Sánchez-Sánchez, R.M. Navarro, J.L.G. Fierro, Catal. Today 129 (2007) 336–345.
[39] X. Hu, D. Dong, L. Zhang, G. Lu, Catal. Commun. 55 (2014) 74–77.
[40] B. Agarski, V. Nikolić, Ž. Kamberović, Z. Anđić, B. Kosec, I. Budak, J. Cleaner Prod. 162 (2017) 7–15.
[41] K. Michalska, P. Kowalik, M. Konkol, W. Próchniak, K. Stołecki, G. Słowik, T. Borowiecki, Appl. Catal. A: Gene 523 (2016) 54–60.
[42] L. Wang, X. Cheng, Z. Wang, C. Ma, Y. Qin, Appl. Catal. B: Environ. 201 (2017) 636–651.
[43] J.S. Moura, M.Od.G. Souza, Md.C. Rangel, Fuel 87 (2008) 3627–3630.
[44] N. Srisiriwat, S. Therdthianwong, A. Therdthianwong, Int. J. Hydrogen Energ. 34 (2009) 2224–2234.
[45] J.S. Cho, S.Y. Lee, H.S. Ju, Y.C. Kang, Appl. Mater. Inter. (2015) 25641–25647.
[46] Z. Boukha, C. Jiménez-González, B. Rivas, J.R. González-Velasco, J.I. Gutiérrez-Ortiz, R. López-Fonseca, Appl. Catal. B: Environ. 158–159 (2014) 190–201.
[47] V. Jorge, M. Carolina, E. Javier, A.J. Miren, B. Javier, G.G. Ana, Int. J. Hydrogen Energy (2014) 12586–12596.
[48] J. Vicente, C. Montero, J. Ereña, Int. J. Hydrogen Energy 39 (2014) 12586–12596.